Intestinal barrier function in the naked mole-rat: an emergent model for gastrointestinal insights

Javier Aguilera-Lizarraga[1]*, Anne Ritoux[1], David C. Bulmer[1], Ewan St. John Smith[1]*

[1] Department of Pharmacology, University of Cambridge, Cambridge, United Kingdom

* To whom correspondence should be addressed: Dr. Javier Aguilera-Lizarraga: ja783@cam.ac.uk; Prof. Ewan St. John Smith: es336@cam.ac.uk.

Abstract:

The intestinal barrier plays a crucial role in homeostasis, both by facilitating absorption of nutrients and fluids, and providing a tight shield to prevent the invasion by either pathogen or commensal microorganisms. Intestinal barrier malfunction is associated with systemic inflammation, oxidative stress, and decreased insulin sensitivity, which may lead to the dysregulation of other tissues. Therefore, a deeper understanding of physiological aspects related to an enhanced barrier function is of significant scientific and clinical relevance. The naked mole-rat has many unusual biological features, including attenuated colonic neuron sensitivity to acid and bradykinin, and resistance to chemical-induced intestinal damage. However, insight into their intestinal barrier physiology is scarce. Here, we observed notable differences in intestinal tissue structure between naked mole-rats and mice. This was characterised by thicker muscularis and submucosa layers, longer villi and larger crypts. Moreover, naked mole-rats showed increased number of larger goblet cells and elevated mucus content. In measuring gut permeability, naked mole-rats showed reduced permeability compared to mice, especially in ileum. Furthermore, intestinal anion secretion induced by serotonin, bradykinin, histamine, and capsaicin was significantly reduced in naked mole-rats compared to mice, despite the expression of receptors for all these agonists. Collectively, these findings indicate that naked mole-rats possess a robust gastrointestinal barrier, that is hard to penetrate and is resistant to environmental and endogenous irritants. Naked mole-rats may therefore provide valuable insights into the physiology of the intestinal barrier related to different pathological conditions and set the stage for the development of innovative and effective therapies.

Keywords: gut; intestinal function; naked mole-rat; intestinal permeability; mucosal anion secretion.

35 **Graphical abstract**:

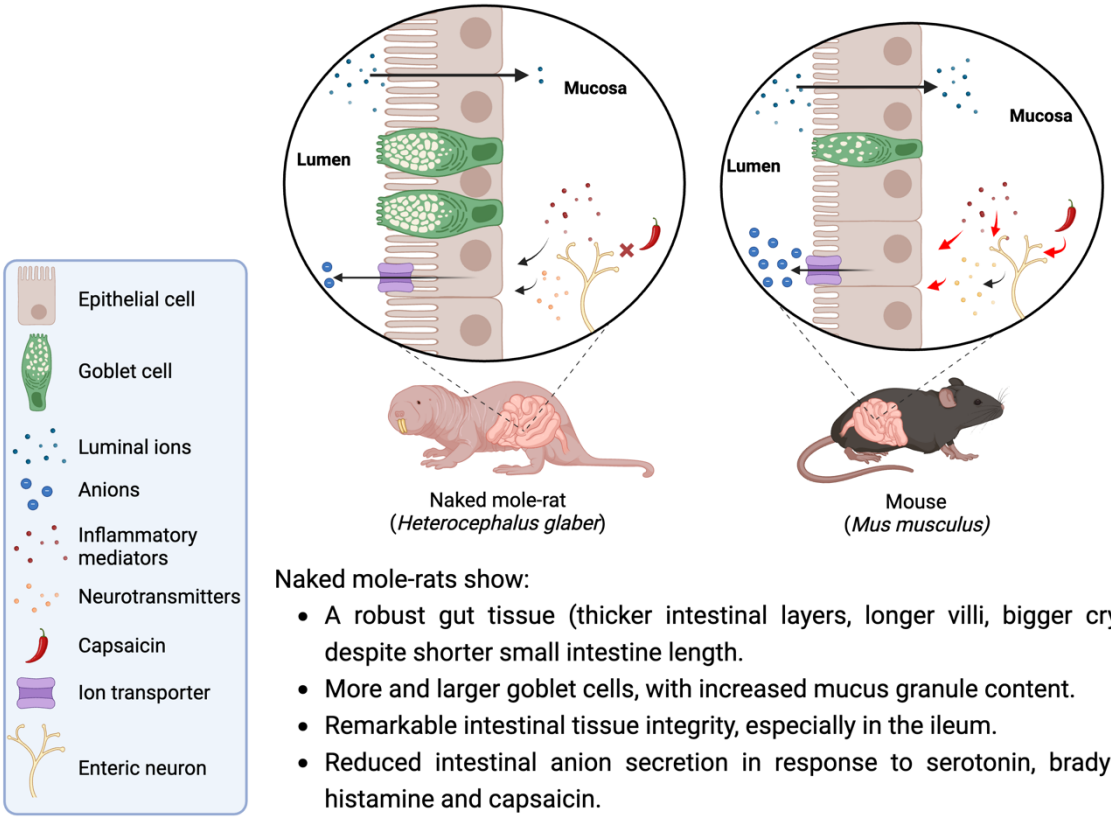

Naked mole-rats show:

- A robust gut tissue (thicker intestinal layers, longer villi, bigger crypts), despite shorter small intestine length.
- More and larger goblet cells, with increased mucus granule content.
- Remarkable intestinal tissue integrity, especially in the ileum.
- Reduced intestinal anion secretion in response to serotonin, bradykinin, histamine and capsaicin.

36

1. Introduction:

Digestive pathologies stand out as the most common type of disease worldwide (*1*). Importantly, they result in a significant reduction in the quality of life for patients and represent a multi-billion healthcare burden globally (*2–5*). Intestinal barrier dysfunction is a common feature of most gastrointestinal diseases, including coeliac disease, inflammatory bowel disease, metabolic dysfunction-associated liver disease and disorders of gut-brain interaction (*6*). Moreover, numerous pathologies unrelated to the gastrointestinal tract, such as respiratory diseases (*7*), skin conditions (*8*) and neurodegenerative diseases (*9*), have also been associated with impaired intestinal barrier function. The common denominator of intestinal barrier perturbation led to the "leaky gut" hypothesis (*10*), which states that enhanced intestinal permeability, caused by endogenous or exogenous factors, may increase the passage of food antigens, commensal microorganisms and/or pathogens into the underlying tissue and the systemic circulation, leading to aberrant immune activation described in different disease conditions. Although increased permeability may not necessarily be deleterious (*11*), and whether intestinal barrier dysregulation is the cause or consequence in most disorders is unknown, it is broadly accepted that adequate functioning of the intestinal barrier is required to maintain gut and inter-organ homeostasis. Consequently, identifying mechanisms leading to enhanced intestinal barrier function is highly relevant for both basic and clinical sciences.

In addition to the use of human intestinal mucosal biopsies (*12*), many models have been employed to investigate the (patho)physiology of the intestinal barrier. Among these, gut-derived cell lines (*13*), such as Caco-2 cell monolayers (*14*), and animal models, primarily rodents, but also porcine, equine and avian models (*15*), have been most commonly utilised. Furthermore, human organoids have recently been implemented to model intestinal epithelial barrier function (*16*, *17*). Despite important advances in our understanding of intestinal barrier function, there has been little to no reduction in the global incidence and prevalence of gastrointestinal conditions over the last 30+ years (*1*). There is thus an imperative need for further research, including the development of novel models, to enhance understanding of intestinal barrier function.

In recent years, naked mole-rats (NMR, *Heterocephalus glaber*) have attracted considerable attention from scientists as a non-traditional animal model due to their highly unusual biological features (*18*). Notably, these animals show an outstanding tolerance to environmental stressors associated with human diseases. Indeed, these eusocial rodents, which have an unusually long lifespan given their 40-80 g size (>35 years) (*19*), have been used for investigating 'healthy' aging (*20*), cancer resistance (*21*), and protection against neurodegeneration (*22*). However, the gastrointestinal tract of these animals remains poorly characterised. Of interest, a recent study revealed that the intestinal barrier of NMRs is resistant to tissue damage induced by dextran sodium sulphate (DSS) (*23*), a widely used colitogenic chemical for modelling inflammatory bowel disease. Although the authors employed a modified version of the traditional DSS protocol (*24*), NMRs displayed no signs of histological damage, even when exposed to 8.75% DSS, albeit for only 3-days. We therefore hypothesised that NMRs would display enhanced intestinal function, that is, improved permeability and resistance to intestinal irritants. To answer this question, we explored the macroscopic and microscopic features of the NMR gut, intestinal permeability, changes in mucosal anion secretion, and expression of intestinal markers of biological interest.

Investigating the intestinal barrier function in NMRs may enable a better understanding of the underlying mechanisms that contribute to better mucosal protection.

2. Material and Methods:

2.1. Animals

All animal experiments were performed in accordance with the Animals (Scientific Procedures) Act 1986 Amendment Regulations 2012 under Project Licenses granted to E.St.J.S. (P7EBFC1B1 and PP5814995) by the Home Office and approved by the University of Cambridge Animal Welfare Ethical Review Body. Experiments were performed using a mixture of male and female C57BL6/J mice (10-15 weeks old; IQR 10-12) and a mixture of male and female, non-breeder, NMRs (23-145 weeks; IQR 48-54). Mice were purchased from Envigo and housed conventionally with nesting material and a red plastic shelter in a temperature-controlled room at 21 °C, with a 12-hour light/dark cycle and access to food and water *ad libitum*. NMRs were bred in-house and maintained in an interconnected network of cages in a humidified (~55%) temperature-controlled room at 28-32 °C with red lighting (08:00−16:00). NMRs had access to food *ad libitum*. In addition, a heat cable provided extra warmth under two to three cages/colony. NMRs used in this study came from five different colonies. Animals were humanely killed by CO_2 exposure followed by cervical dislocation (mice) or decapitation (NMRs).

2.2. Intestinal tissue processing for histology and histomorphometric assessment

Intestinal biopsies (ileum and colon) were fixed and embedded using conventional techniques. In brief, samples were incubated, after dissection, in 4% paraformaldehyde (PFA) at 4 °C overnight. Next, samples were washed in PBS, transferred to sucrose ($0.3\ g \cdot ml^{-1}$) and stored at 4 °C overnight. Finally, samples were embedded in Shandon M-1 Embedding Matrix (Thermo Fisher Scientific), snap-frozen and stored at −80°C until processing. Cryostat (Leica) sections (12 µm) were collated across Superfrost Plus slides (Thermo Fisher Scientific) and stained with haematoxylin and eosin (H&E) using conventional techniques (*25*, *26*). Villi length and width, crypts length and width, and thickness of the different layers (submucosa and muscularis) were measured in ileum and colon samples (Supplementary Figure 1a, b) using ImageJ software. For analyses of villi and crypts, only intestinal units that were overtly complete and full-sized, and showed no signs of bending or mechanical damage, were chosen in each sample. A total of 5-10 units of each kind were carefully selected, and their average calculated.

2.3. Alcian blue/periodic acid-Schiff (AB/PAS) staining

For goblet cell identification and quantification of their mucus content, 12-µm tissue sections were subjected to Alcian Blue and Periodic Acid Schiff's (AB/PAS) staining. In brief, sections were hydrated in double distilled water and then stained with Alcian Blue solution (Sigma, 1% w/v Alcian Blue in 3% v/v aqueous acetic acid) for 15 minutes. Next, sections were rinsed in double distilled water before being treated for 5 minutes with 0.5% periodic acid (Sigma). Thereafter, tissue sections were washed again in double distilled water and stained for 10

minutes in Schiff's reagent (Sigma). Finally, sections were washed for 5 minutes in tap water, mounted, and imaged using a NanoZoomer S360 (Hamamatsu).

For analyses, images were loaded into the QuPath software (*27*). In each image, regions of interest (ROI) for crypts and villi were manually annotated. Within these, the cell detection tool was used to segment individual cells using a manually selected threshold. To ensure that the segmentation correctly circled cells, ROIs were visually inspected. After colour deconvolution, measurements for average pixel intensity across each cell ROI and cell area were analysed.

2.4. Ussing chambers

Post-mortem, for both species, the gastrointestinal tract (from pyloric sphincter to anus) was carefully removed, cleaned of faecal pellets, and maintained in ice-cold Krebs solution. For experiments where transepithelial electrical resistance (*TEER*) was measured, full-thickness segments of ileum and colon were mounted in Ussing chambers without removal of the muscularis propria or the serosa. For experiments where short-circuit current (I_{sc}) was measured, ileum samples were pinned in Sylgard plates with the lamina propria facing down and muscularis externa and serosal layers gently peeled off with forceps to prepare lamina propria-submucosal plexus intestinal strips. Multichannel DVC 1000 Voltage/Current clamp apparatus (World Precision Instruments) was used to measure changes in intestinal tissue function. Each channel was connected to a DVC-3 preamplifier (World Precision Instruments), connected to two current and two voltage electrodes filled with 1.5% (w/v) agar (Millipore) dissolved in 3M KCl. The voltage and fluid resistance were zeroed to eliminate electrical bias and the voltage clamp circuitry was set to standby mode and the intestinal preparation was mounted in the chamber with fresh superfusate. After calibration, intestinal tissues were then mounted in Ussing chambers and the mucosal and serosal compartments were bathed independently with 10 mL of Krebs-Ringer bicarbonate buffer (pH 7.4) containing (in mM): 118 NaCl; 4.7 KCl; 1.2 $CaCl_2$; 1.2 $MgSO_4$; 1.2 NaH_2PO_4; 25 $NaHCO_3$). Glucose (10 mM) was present in the medium that bathed the serosal surface of the tissue and mannitol (10 mM) was substituted for glucose in the medium that bathed the mucosal surface. Media were oxygenated (95% O_2, 5% CO_2) throughout the experiment via a gas-uplift recirculation system and maintained at 37˚C by water-jacketed reservoirs. Although NMRs are cold blooded and maintained at 28-32 °C, to minimise the number of variables impacting our results, all experiments were conducted with media maintained at 37 °C. For mouse tissue, Ussing chambers with an exposed area of 0.071 cm^2 were used, while an exposed area of 0.196 cm^2 was used for NMR tissue.

Transepithelial electrical resistance (TEER) experiments: The transepithelial electrical resistance was calculated according to Ohm's law (resistance = voltage/current, normalised by the exposed window area; TEER = $R_{tissue}(\Omega) \cdot \text{Area } (mm^2)$) from the voltage deflections induced by bipolar current pulses of 50 µA every 50 s with a duration of 500 ms. After 30 min of tissue stabilisation, TEER was measured over a period of 2 h.

Short-circuit current (I_{sc}) *experiments*: After mounting, tissue was allowed to equilibrate for 15-20 min. Thereafter, preparations were short-circuited (voltage-clamped at zero potential) and the short-circuit current (I_{sc}) required to maintain the 0 mV potential was monitored over time. After short-circuiting, intestinal tissue allowed to equilibrate for 10-15 min to allow bioelectric measures to stabilise (baseline). All I_{sc} responses were normalised to $\mu A \cdot cm^{-2}$ and changes in I_{sc} (ΔI_{sc}) were recorded after application of compounds to the serosal side.

170

171 ***2.5. Chemicals***

172 The following drugs were used for short-circuit current (I_{sc}) experiments: capsaicin (Sigma-
173 Aldrich), bradykinin (Tocris), 5-hydroxytryptamine (5-HT, serotonin) (Sigma-Aldrich) and
174 histamine (Sigma-Aldrich). Capsaicin (1 mM) was dissolved in 100% ethanol and bradykinin
175 (1 mM), 5-HT (10 mM) and histamine (10 mM) were dissolved in double distilled water.

176

177 ***2.6. RNA extraction from intestinal tissue and cDNA preparation***

178 Following dissection and cleaning, intestinal samples (ileum and colon) were stored in
179 RNAprotect Tissue Reagent (Qiagen) at 4˚C until processing. Next, total RNA was isolated
180 using the RNeasy Mini Kit (Qiagen) following the manufacturer's instructions and including a
181 DNase digestion step. Subsequently, cDNA was transcribed using qScript cDNA Synthesis Kit
182 (Quantabio) following the manufacturer's instructions.

183

184 ***2.7. Real-time quantitative PCR (RT-qPCR):***

185 Reactions were prepared with FastStart Sybr Green Master (Merk) following the
186 manufacturer's instructions. In brief, 10 µL reaction mix per well, containing cDNA (20 ng)
187 oligonucleotides (200 nM) and UltraPure distilled water (DNase/RNase free; Invitrogen), were
188 loaded onto 96-well plates. Thermocycling was performed using a StepOnePlus™ Real-Time
189 PCR System (Thermo Fisher). A melt curve was performed at the end of thermocycling to
190 assess the specificity of primers. Single peaks were obtained for all primer pairings.

191 To determine primer efficiency, a standard curve was generated for each pair of primers at
192 cDNA concentrations of 50, 5, 0.5, 0.05 and 0.005 ng/µL and plotting C_t against log
193 concentration. Efficiency was calculated by the following equation: Efficiency = $10^{-(1/slope)}$-1
194 (*28*, *29*). Efficiency of reaction values between 90 and 110% were considered acceptable.

195 Gene expression was normalised to the endogenous reference gene *Tbp* for both species.
196 This gene encodes the TATA-binding protein. *Tbp* was chosen as it has been proposed as an
197 ideal reference gene for the normalisation of gene expression in intestinal samples of mice
198 and other animals (*30*–*34*). Relative gene expression was calculated as $2^{-\Delta\Delta Ct}$ (*35*). The primer
199 pairs used are described in Supplementary Table 1.

200

201 ***2.8. Biotinylated hyaluronan binding protein staining*:**

202 Biotinylated hyaluronan binding protein (HABP) staining was performed as previously
203 described (*25*). In brief, 12 µm intestinal tissue sections were washed 3 times in PBS-Tween20
204 and subsequently blocked for 1 hour in a diluent solution (0.2% Triton X-100 and 5% bovine
205 serum albumin in PBS). Slides were then incubated overnight with HABP (Amsbio) in the
206 diluent (1:200) at 4 °C. Next, the slides underwent another round of washing with PBS-
207 Tween20 and were incubated for 2 hours at room temperature with streptavidin conjugated to
208 AlexaFluor 488 (Invitrogen). After three final washes with PBS-Tween20, glass coverslips
209 were mounted onto the slides using MOWIOL mounting medium (Sigma-Aldrich). Samples
210 were imaged using an Olympus BX51 microscope and QImaging camera.

211

2.9. Measurement of Substance P from intestinal explants

Post-mortem, the small intestine and colon were carefully removed, cleaned of faecal pellets and maintained in ice-cold Krebs solution. Next, 30-50 mg tissue sections (terminal ileum and distal colon) were dissected and transferred into 24-well plates containing 500 µL per well of L-15 Medium (GlutaMAX) medium (Gibco). Explants from both species were incubated for 5 min at 32 °C (5% CO_2, 3%O_2). Thereafter, culture supernatant was collected and stored at -80˚C until use. Substance P was measured using an enzyme-linked immunosorbent assay (Substance P ELISA Kit, Cayman Chemicals) according to the manufacturer's instructions. Substance P levels were normalised to protein content upon quantification using the Bradford Assay (Thermo Fisher) following the manufacturer's instructions.

2.10. Statistical analyses:

Tissue was taken from non-manipulated healthy animals being used for other experiments, thus meeting the Reduction aim of the 3Rs. While there were no upfront power calculations to determine the sample size, we included sample sizes commonly used for the types of assays used in this study (*36*, *37*).

Normal (Gaussian) distribution was determined for all datasets using the Shapiro–Wilk normality test. Non-parametric tests were used for datasets where ≥1 group did not pass the normality test (assuming $\alpha = 0.05$). Otherwise, parametric tests were used. The type of statistical test and the sample sizes for each experiment are provided in figure legends. Data were plotted and statistical analyses performed with Prism (GraphPad Software version 10.2.1). A *p*-value <0.05 was considered statistically significant. Finally, effect sizes were calculated post *hoc* using the statistical software G*Power (Version 3.1.9.6).

For histological assessment of mouse and NMR samples, 2-4 sections per animal, separated by at least 150 µm, were randomly captured, and analysed by an experimenter in a blinded manner. The experimenter was unblinded for statistical analysis.

3. **Results**:

3.1. Macroscopic features of the naked mole-rat gastrointestinal tract.

NMRs are small rodents whose body mass is significantly larger compared to mice (data from this study: mouse 21.05 ± 1.71 g vs. NMR 47.49 ± 13.28 g, $p < 0.0001$, Figure 1a), yet substantially smaller than typically used laboratory adult rats (Sprague-Dawley, ~300-400 g; Wistar rats, ~250-500 g) (*38*, *39*) or guinea pigs (Hartley, ~625-1,200 g) (*40*). Despite the larger size of NMRs compared to mice, NMRs showed a noticeably shorter gut length, measured from the pyloric sphincter to the anus (mouse 40.09 ± 2.35 cm vs. NMR 22.17 ± 1.94 cm, $p < 0.0001$; Figure 1b, c). Further analyses revealed that these differences were driven by a shorter small intestine in NMR than that of mice (small intestine: mouse 32.69 ± 1.92 cm vs. NMR 14.95 ± 1.88 cm, $p < 0.0001$; colon: mouse 7.40 ± 0.65 cm vs. NMR 7.28 ± 0.59 cm, $p = 0.6425$; Figure 1d, e), in keeping with previous studies (*23*, *41*). Of interest, while the ratio of the small intestine/colon length in mice was comparable to that in humans (*42*–*44*), this was reduced by ~2-fold in NMRs (human 3.956 ± 1.36 vs. mouse 4.52 ± 0.99 vs. NMR 2.07 ± 1.20, $p < 0.0001$; Figure 1f). The lengths of the NMR small intestine and colon were comparable between male and female (small intestine: male 15.50 ± 6.60 cm vs. female

15.05 ± 2.50 cm, p = 0.5626; colon: male 7.10 ± 2.00 cm vs. female 7.55 ± 0.20 cm, p = 0.2265; Supplementary Figure 1c, d). Given the considerable age range of the NMRs used in our study (minimum age: 23 weeks old; maximum age: 145 weeks old) and their attainment of adulthood at ~1 year old, we analysed the relationship between gut length and both age and weight. The colon length was not associated with the age or weight of the NMR (age vs. length: r = 0.0581, p = 0.8248, weight vs. length: r = 0.0245, p = 0.9339; Supplementary Figure 1e, f). However, we did find statistically significant correlations between the small intestine length and the age and weight of NMRs (age vs. length: r = 0.7293, p = 0.0012, weight vs. length: r = 0.6258, p = 0.0282; Supplementary Figure 1g, h). These findings parallel human anatomical data, that is, the length of the colon in young/adolescent individuals is similar to that in adults (*45*), while the small intestine only reaches its maximum length in adulthood (*46*). Overall, these results show gross anatomical differences in the gut of NMRs compared to humans and mice, especially regarding the short length of the small intestine.

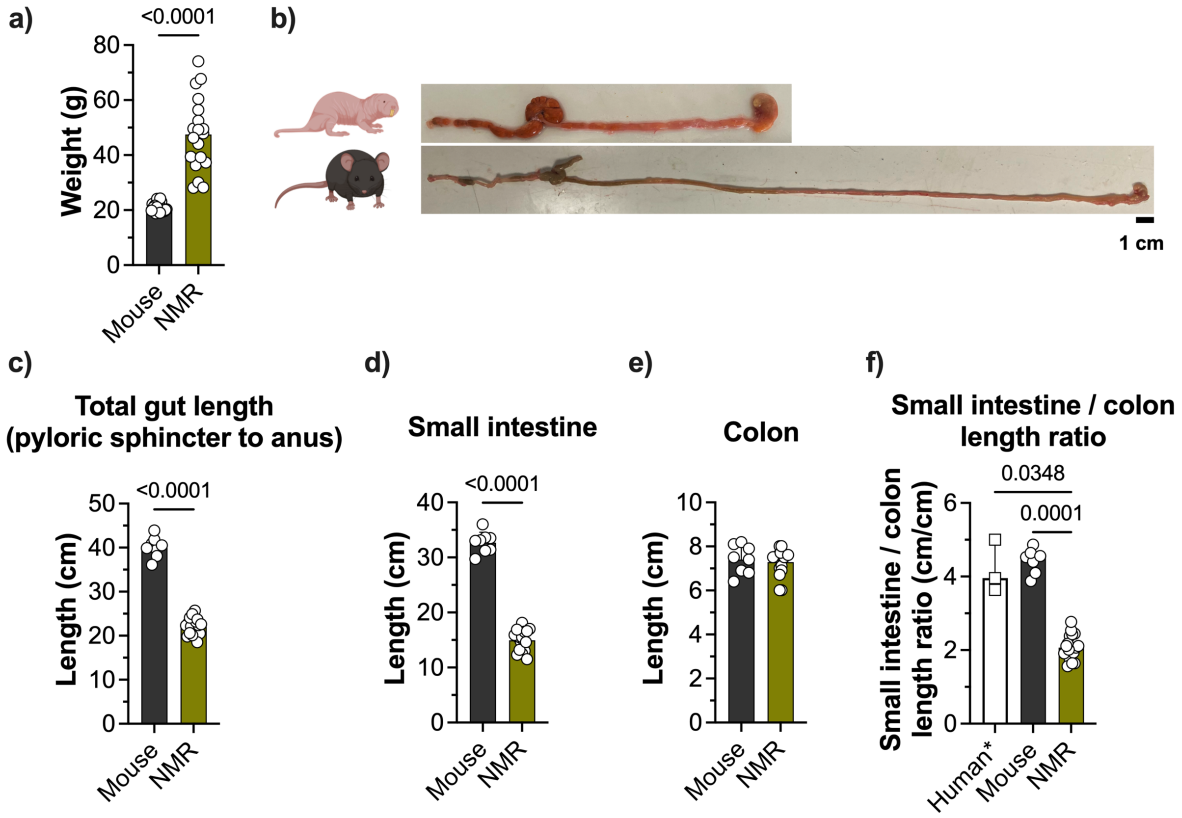

Figure 1. Anatomical features of gastrointestinal tracts of NMRs compared to mice. Weight of mice (n = 20) compared to NMR (n = 19) (**a**). **b**, Representative pictures of the gastrointestinal tract (from stomach to anus) of NMR (upper panel) and mouse (lower panel). Gastrointestinal length measured from the pyloric sphincter to the anus (**c**), small intestine (**d**) and colon (**e**) in mice (n= 8) and NMRs (n = 17). **f)** Length ratio of the small intestine compared to the colon in humans (data extracted from *(*42–44*)*), mice and NMR. Human* data reflect median of the means provided by 3 studies that analysed 100, 100 and 200 individuals, respectively. *P* values are shown in plots. **c**, **d** and **e**, unpaired t-test (data shown as mean ± SD); **f**, Kruskal-Wallis test followed by Dunn's multiple comparisons test (data shown as median ± IQR). The NMR and mouse illustrations in **a** were created with BioRender.com).

3.2. Intestinal histology in naked mole-rats

Next, we explored the microscopic architecture of the small intestine (ileum) and colon in NMRs, comparing them to those of mouse tissue (Figure 2a-d). To this end, we measured the

histological properties of the intestinal villi and crypts, as well as the thickness of different layers. The ileum of NMRs showed thicker muscularis (mouse 37.56 ± 8.24 μm vs. NMR 60.45 ± 23.43 μm, $p = 0.0055$; Figure 2e) and submucosal layers compared to mice (mouse 18.90 ± 2.02 μm vs. NMR 40.46 ± 11.22 μm, $p < 0.0001$; Figure 2f). Furthermore, NMR ileal villi were substantially longer (mouse 344.4 ± 180.8 μm vs. NMR 801.0 ± 394.3 μm, $p < 0.0001$; Figure 2g) and wider (mouse 90.95 ± 10.00 μm vs. NMR 135.3 ± 36.63 μm, $p = 0.0008$; Figure 2h) compared to those of mice, and NMR ileal crypts were significantly deeper (mouse -135.60 ± 66.81 μm vs. NMR -157.10 ± 47.49 μm, $p = 0.0039$; Figure 2i) and wider (mouse 35.72 ± 6.45 μm vs. NMR 57.86 ± 10.39 μm, $p < 0.0001$; Figure 2j). In the colon, the muscularis was comparable in both species (mouse 128.2 ± 78.31 μm vs. NMR 139.3 ± 83.82 μm, $p = 0.2188$; Figure 2k), but the colonic submucosa was thicker in NMRs (mouse 63.13 ± 10.18 μm vs. NMR 80.27 ± 10.26 μm, $p = 0.0012$; Figure 2l). Finally, colonic crypts were similarly deep in both species (mouse -219.0 ± 32.57 μm vs. NMR -198.0 ± 12.64 μm, $p = 0.0837$; Figure 2m), but those of NMRs were significantly wider compared to mice (mouse 34.07 ± 3.35 μm vs. NMR 56.79 ± 7.24 μm, $p < 0.0001$; Figure 2n).

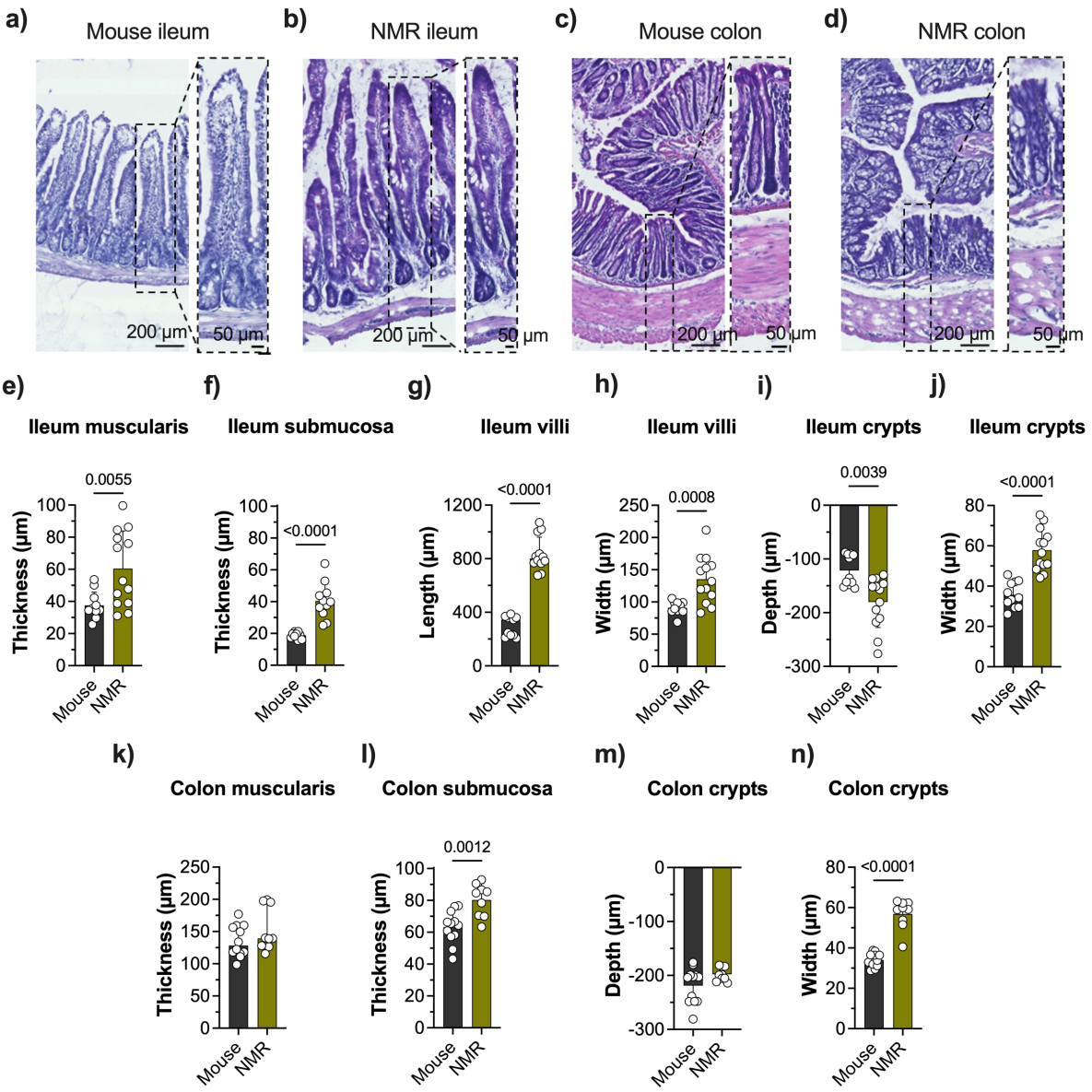

Figure 2. Intestinal histology in NMRs. Representative images of H&E staining sections from mouse (**a**) and NMR (**b**) ileum, and mouse (**c**) and NMR (**d**) colon. Ileum muscularis (**e**) and submucosal (**f**) layers thickness in mouse (n = 11, 2-3 sections/animal, 4 mice) and NMR (n = 13, 3-4 sections/animal, 4 NMR). **g**, average villi height (5-10 villi/sample) in mice (n = 11, 2-3 sections/animal, 4 mice) and NMRs (n = 12). **h**, average villi width (5-10 villi/sample) in mice (n = 11, 2-3 sections/animal, 4 mice) and NMRs (n = 13, 3-4 sections/animal, 4 NMR). **i**, average crypt depth (5-10 crypts/sample) in mice (n = 11, 2-3 sections/animal, 4 mice) and NMRs (n = 13, 3-4 sections/animal, 4 NMR). **j**, average crypt width (5-10 crypts/sample) in mice (n = 11) and NMRs (n = 13). Colon muscularis (**k**) and submucosal (**l**) layers thickness in mouse (n = 12, 3 sections/animal, 4 mice) and NMR (n = 9, 3 sections/animal, 3 NMRs). **m**, average crypt depth (5-10 crypts/sample) in mice (n = 12, 3 sections/animal, 4 mice) and NMRs (n = 9, 3 sections/animal, 3 NMRs). **n**, average crypt width (5-10 crypts/sample) in mice (n = 12, 3 sections/animal, 4 mice) and NMRs (n = 9, 3 sections/animal, 3 NMRs). *P* values are shown in plots. **e**, **f**, **h**, **j**, **l**, **m** and **n**, unpaired t-test (data shown as mean ± SD); **g**, **i** and **k**, Mann-Whitney test (data shown as median ± IQR).

We next used Alcian Blue/Periodic Acid-Schiff (AB/PAS) staining to identify goblet cells and quantify mucus granule content in small intestine and colon samples. Ileum samples (Figure 3a, b) of NMR showed similar numbers of AB^+ mucin-producing goblet cells in the villi compared to mice (mouse 80.07 ± 23.25 cells/villus vs. NMR 93.07 ± 20.41 cells/villus, p = 0.2254; Figure 3c), and slightly higher numbers in the crypts (mouse 28.66 ± 7.97 cells/crypt vs. NMR 38.98 ± 8.86 cells/crypt, p = 0.0194; Figure 3c). However, the size of the goblet cells

present in the NMR ileum was significantly larger than that of mouse ileum goblet cells, both in the villi and crypts (mouse villi 33.91 ± 3.42 μm^2 vs. NMR villi 41.79 ± 7.62 μm^2, $p = 0.012$; mouse crypts 29.25 ± 3.71 μm^2 vs. NMR crypts 46.53 ± 5.79 μm^2, $p < 0.0001$; Figure 3d). In addition, the goblet cell-mucus granule content (measured as AB/PAS staining intensity per cell) in NMR ileum, in both villi- and crypts-residing cells, was significantly higher compared to that of mice (mouse villi 0.51 ± 0.04 a.u. vs. NMR villi 0.74 ± 0.10 a.u., $p < 0.0001$; mouse crypts 0.48 ± 0.06 a.u. vs. NMR crypts 0.89 ± 0.12 a.u., $p < 0.0001$; Figure 3e). In the colon (Figure 3f, g), the number of AB$^+$ goblet cells was significantly elevated in the crypts of NMR compared to in mice (mouse 14.07 ± 1.51 cells vs. NMR 23.97 ± 4.54 cells, $p < 0.0001$; Figure 3h). Furthermore, as in the ileum, the size of these goblet cells was significantly bigger in NMR compared to mice (mouse crypts 65.98 ± 14.77 μm^2 vs. NMR crypts 170.2 ± 21.43 μm^2, $p < 0.0001$; Figure 3d). Finally, again, in keeping with the results obtained in the ileum, the mucus granule content in NMR colonic crypts was significantly larger than that of mouse colonic crypts (mouse 1.00 ± 0.05 a.u. vs. NMR 1.42 ± 0.19 a.u., $p < 0.0001$; Figure 3j).

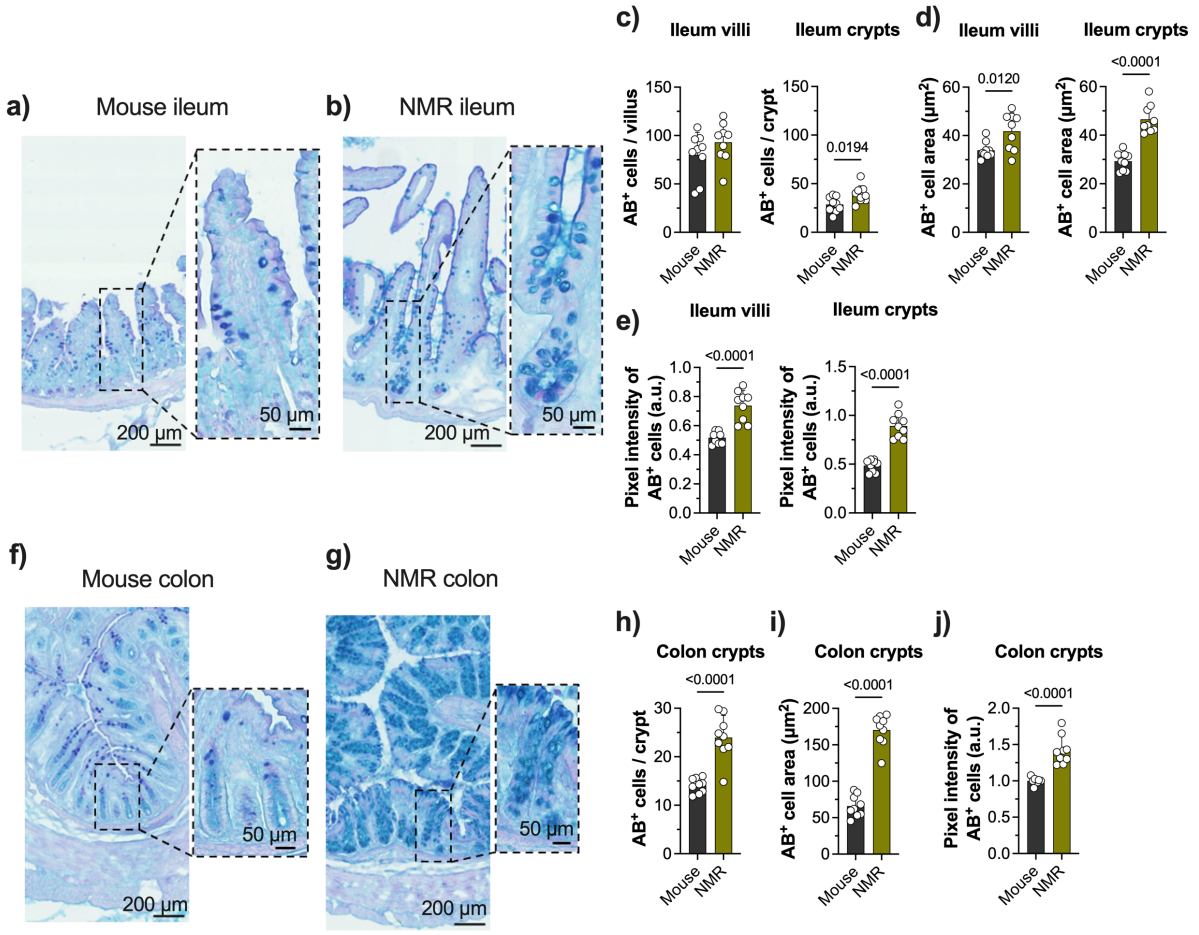

Figure 3. Goblet cells and mucus content in the gut of NMRs. Representative images of mouse (**a**) and NMR (**b**) ileum samples stained with AB/PAS. **c**, number of AB$^+$ cells (goblet cells) in the ileum villi (left) and crypts (right) in mice (n = 9, 3 sections/animal, 3 mice) and NMRs (n = 9, 3 sections/animal, 3 NMRs). **d**, area of AB$^+$ cells in the ileum villi (left) and crypts (right) in mice (n = 9, 3 sections/animal, 3 mice) and NMRs (n = 9, 3 sections/animal, 3 NMRs). **e**, pixel intensity measurement AB/PAS staining in the ileum villi (left) and crypts (right) in mice (n = 9, 3 sections/animal, 3 mice) and NMRs (n = 9, 3 sections/animal, 3 NMRs). Representative images of mouse (**f**) and NMR (**g**) colon samples stained with AB/PAS **h**, number of AB$^+$ cells in the colon crypts in mice (n = 9, 3 sections/animal, 3 mice) and NMRs (n = 9, 3 sections/animal, 3 NMRs). **i**, area of AB$^+$ cells in crypts in mice (n = 9, 3 sections/animal, 3 mice) and NMRs (n = 9, 3 sections/animal, 3 NMRs). **j**, pixel intensity measurement AB/PAS staining in colon crypts in mice (n = 9, 3 sections/animal, 3 mice) and NMRs (n = 9, 3 sections/animal, 3 NMRs). *P* values are shown in plots. **c**, **d**, **e**, **h**, **i** and **j**, unpaired t-test (data shown as mean ± SD).

Altogether, these findings indicate that, despite having a shorter small intestine, the NMR ileum exhibits features that maximise the surface area for nutrient and water absorption, and ionic transport, such as ~2.5-fold larger villi compared to mice (Cohen's d size effect = 5.3). Additionally, the larger crypts found in NMRs may be reflective of differences in tissue turnover in these animals compared to mice. Furthermore, NMR show increased numbers of larger goblet cells both in the ileum and in the colon, with a significantly higher mucus content compared to murine goblet cells. This likely confers enhanced protection upon these animals against the infiltration of microorganisms, digestive enzymes and acids, digested food particles, as well as luminal by-products and toxins.

3.3. Intestinal integrity: ileum and colon.

Because of the clear differences in NMR intestinal structures compared to those of mice, we next aimed to examine the physical properties of this tissue. To this end, we used the gold standard technique for this purpose, i.e., the Ussing chamber for measuring mucosal membrane properties. We measured the transepithelial electrical resistance (TEER), as a measure of intestinal barrier integrity. High TEER values are indicative of decreased permeability to ions. Interestingly, the NMR terminal ileum showed a remarkably higher TEER, i.e. reduced permeability, compared to the mouse terminal ileum (mouse 45.41 ± 19.71 $\Omega \cdot cm^2$ vs. NMR 148.6 ± 67.28 $\Omega \cdot cm^2$, $p = 0.0012$; Cohen's *d* size effect = 7.15; Figure 4a, b). The NMR distal colon also showed reduced permeability compared to the mouse distal colon, but the difference was less pronounced (mouse 52.35 ± 20.27 $\Omega \cdot cm^2$ vs. NMR 74.53 ± 16.68 $\Omega \cdot cm^2$, $p = 0.0012$; Cohen's *d* size effect = 2.59; Figure 4c, d). While the terminal ileum in mice exhibited greater permeability compared to their colon (ileum 45.41 ± 19.71 $\Omega \cdot cm^2$ vs. colon 52.35 ± 20.27 $\Omega \cdot cm^2$, $p = 0.0197$; Cohen's *d* size effect = 1.24; Supplementary Figure 2a), which aligns with prior studies in mice (*47*) and is also noted in rats (*48*, *49*) and humans (*49*, *50*), the terminal ileum of NMRs was extraordinarily less permeable than their distal colon (ileum 148.6 ± 67.28 $\Omega \cdot cm^2$ vs. colon 74.53 ± 16.68 $\Omega \cdot cm^2$, $p = 0.0043$; Cohen's *d* size effect = 5.34; Supplementary Figure 2b). Altogether, these results indicate that the integrity of the gastrointestinal tract in NMRs is increased compared to mice, with the NMR small intestine (ileum) showing a strikingly low tissue permeability.

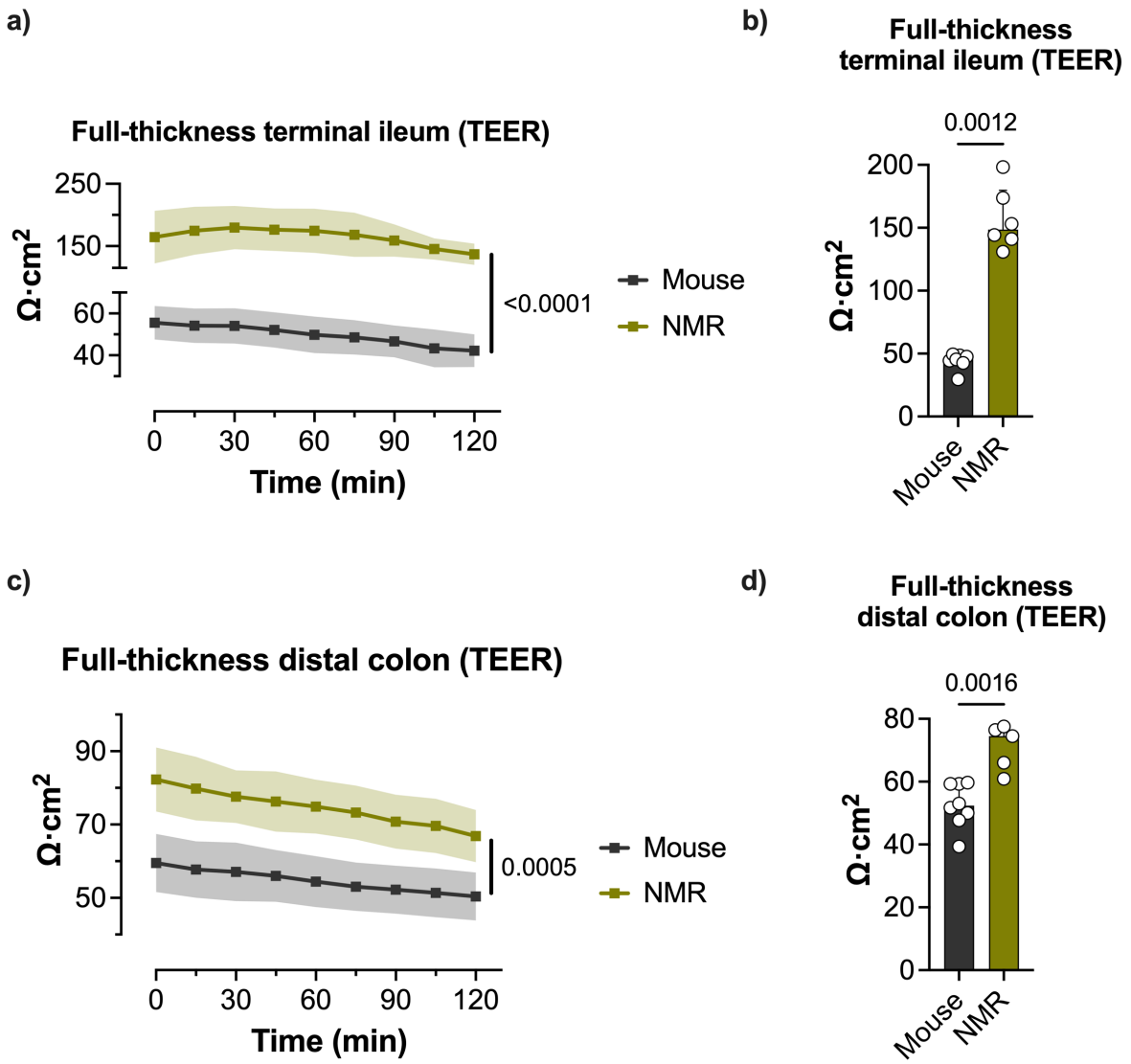

Figure 4. Increased intestinal permeability in NMR. a, **b)** transepithelial electrical resistance (TEER) in the terminal ileum of mice (n = 7) and NMRs (n = 8). **c**, **d)** TEER in the distal colon of mice (n = 8) and NMRs (n = 5). Data in **b** and **d** were calculated as the average TEER values between 60 min and 120 min and plotted as individual values. *P* values are shown in plots. **a**, **c**, 2-way ANOVA and Šidak's multiple comparison test (data shown as mean, shadow area represents the SD); **b**, **d**, Mann-Whitney test (data shown as median ± IQR).

3.4. Anion transport in the terminal ileum.

Given the different mucosal integrity properties observed in NMR vs. mouse ileal tissue, we next utilised this region to assess intestinal anion secretion. To this end, we measured the short-circuit current (I_{sc}), as this reflects the net ionic transport, mainly Cl^- and Na^+ in the small intestine, through the mucosa (*6*). An increase in I_{sc} is primarily attributable to anion secretion to the intestinal lumen. We selected four compounds known to evoke anion secretion in rodents and/or humans, such as 5-hydroxytryptamine (5-HT, serotonin) (*51*, *52*), bradykinin (*53*, *54*), histamine (*55*, *56*) and capsaicin (*57*, *58*). In keeping with previous studies, we confirmed that 5-HT, bradykinin, histamine, and capsaicin evoke a prominent anion secretion to the ileal mucosa in mice (Figure 5a-d). By contrast, ileum preparations from NMRs showed markedly reduced responses to 5-HT (mouse 179.8 ± 58.15 $\Delta\mu A \cdot cm^{-2}$ vs. NMR 13.23 ± 17.41 $\Delta\mu A \cdot cm^{-2}$, $p < 0.0001$; Figure 5a) and bradykinin (mouse 78.64 ± 22.04 $\Delta\mu A \cdot cm^{-2}$ vs. NMR

17.98 ± 17.05 ΔμA · cm^{-2}, $p < 0.0001$; Figure 5b), and were virtually unresponsive to histamine (mouse 22.28 ± 24.93 ΔμA · cm^{-2} vs. NMR 3.08 ± 3.16 ΔμA · cm^{-2}, $p = 0.0006$; Figure 5c) and capsaicin (mouse 42.56 ± 20.20 ΔμA · cm^{-2} vs. NMR -0.74 ± 1.98 ΔμA · cm^{-2}, $p = 0.0002$; Figure 5d). These results indicate that NMRs display a pronounced resistance to intestinal anion secretion in response to some neurotransmitters, inflammatory mediators, and chemical irritants.

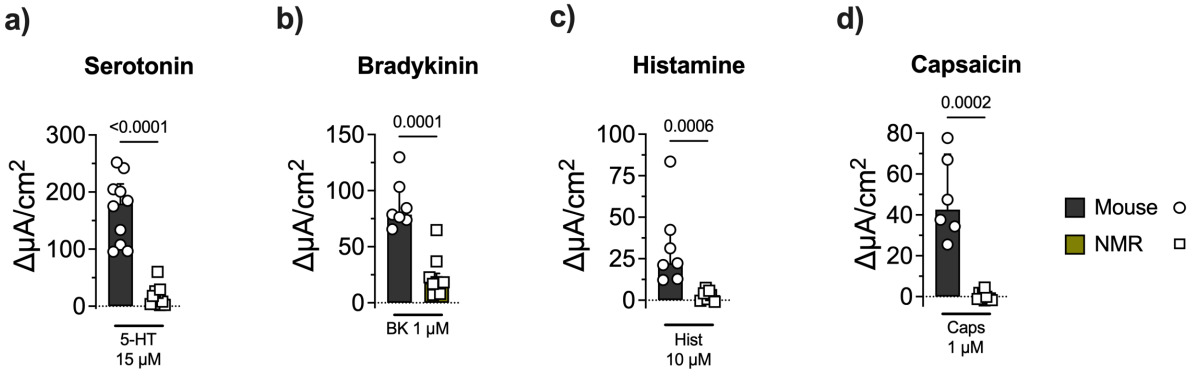

Figure 5. Reduced anion secretion responses in NMRs. a) Short-circuit current increase (ΔI_{sc}) in response to 5-HT in mice (n = 10) and NMRs (n = 11). **b**) ΔI_{sc} in response to bradykinin in mice (n = 10) and NMRs (n = 11). **c**) ΔI_{sc} in response to histamine in mice (n = 7) and NMRs (n = 7). **d**) ΔI_{sc} in response to capsaicin in mice (n = 6) and NMRs (n = 10). For clarity, circles refer to mouse samples and squares to NMRs samples. P values are shown in plots. All data were analysed with Mann-Whitney test (data shown as median ± IQR).

3.5. Expression of receptors involved on intestinal anion transport.

Because NMRs showed altered anion secretion responses to 5-HT, bradykinin, histamine, and capsaicin, we next asked whether NMRs express receptors for these compounds in their intestinal tract. To this end, we used RT-qPCR to evaluate the gene expression of ion channels and receptors associated to these agonists. Importantly, some of these substances can activate several receptors (such as 5-HT, bradykinin, and histamine). Hence, we selected genes that encode receptors known to be involved in intestinal anion secretion in humans and/or rodents. Thus, we assessed the gene expression of the 5-HT receptor 4 (*Htr4*) (*51*), the bradykinin receptor B_2 (*Bdkrb2*) (*53*), histamine H_1 receptor (*Hrh1*) (*56*) and the capsaicin receptor, transient receptor potential vanilloid 1 (*Trpv1*). Notably, both the terminal ileum and the distal colon of NMR expressed all the genes evaluated. Ileum samples from NMR showed a reduced gene expression compared to mouse of *Bdkrb2* (mouse 0.014 ± 0.039 relative expression vs. NMR 0.001 ± 0.007 relative expression, $p = 0.0002$; Figure 6) and *Hrh1* (mouse 0.11 ± 0.73 relative expression vs. NMR 0.007 ± 0.022 relative expression, $p = 0.0003$; Figure 6), whereas similar levels of these genes were expressed in the colon of both species (*Bdkrb2*: mouse 0.01 ± 0.02 relative expression vs. NMR 0.01 ± 0.07 relative expression, $p = 0.7984$; *Hrh1*: mouse 0.01 ± 0.008 relative expression vs. NMR 0.01 ± 0.005 relative expression, $p = 0.2220$; Figure 6). By contrast, colon tissue of NMRs displayed a lower expression of *Htr4* compared to mice (mouse 0.14 ± 0.33 relative expression vs. NMR 0.01 ± 0.03 relative expression, $p = 0.0002$; Figure 6), although no such statistical difference was observed in the ileum across species for *Htr4* (mouse 0.04 ± 0.26 relative expression vs. NMR 0.18 ± 0.42 relative expression, $p = 0.2785$; Figure 6). These results indicate that, while changes in the gene expression of these receptors could partially account for the altered intestinal ion secretion observed in response to some of the compounds evaluated, NMRs express

430 receptors for all these agents along their gastrointestinal tract. Further studies are needed to
431 characterise intestinal secretory responses in these animals.

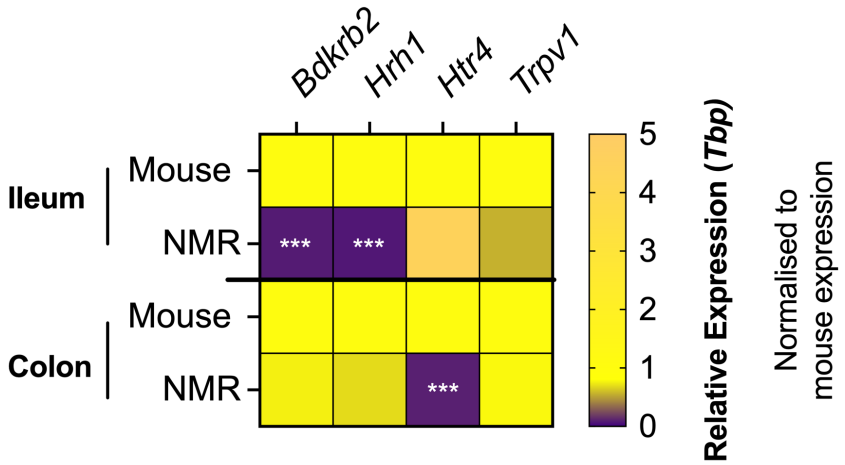

432

433 **Figure 6. Intestinal gene expression of receptors associated with increased anion secretion.** Heatmap of
434 the relative gene expression in terminal ileum and distal colon samples in mice (n = 8) and NMRs (n = 8). All data
435 were analysed with Mann-Whitney test (data shown as colour gradient scale of the relative expression). Each row
436 represents the median of the side-by-side replicates. ***$P < 0.001$.

437

438 ***3.6. Intestinal biomolecules in the gut of naked mole-rats***

439 Finally, we aimed to evaluate biomolecules that have been highlighted to positively contribute
440 to the unusual physiological features found in NMRs. Amongst these, we first focused on
441 hyaluronan, which is an abundant and crucial element in the extracellular matrix of most
442 tissues, including the intestine. This polymer plays a vital role in almost all areas of biology
443 (*59*), including development, tissue architecture, cell proliferation, inflammation, cell migration,
444 etc. Notably, in NMRs, increased levels of hyaluronan can be found in the skin, muscles and
445 lymph nodes (*60*, *61*), NMR hyaluronan also displaying a highly folded structure and being
446 able to form gels without the need for chemical crosslinking (*62*). However, hyaluronan levels
447 and localisation in the NMR intestine have not been characterised. To evaluate this, we used
448 specific biotinylated hyaluronan binding protein (HABP) staining. Of note, aside from gross
449 histological dissimilarities discussed above, no marked differences were observed in either
450 the ileum or the colon of NMRs compared to mice (Figure 7a).

451 Another set of molecules that has garnered considerable interest in NMR is neuropeptides.
452 NMRs do not express substance P and calcitonin gene-related peptide (CGRP) in cutaneous
453 C-fibres (*63*), in contrast to other mammalian species, including mice. Nevertheless, NMRs do
454 produce both substance P and CGRP in longitudinal lanceolate endings associated with
455 follicle-sinus complexes and body hair follicles (*63*), likely through Aβ-fibres. In keeping with
456 this, we previously observed $CGRP^+$ fibres in myenteric neurons in the colorectum of NMR
457 (*41*). Therefore, we asked whether substance P is also synthetised in the NMR gut. To this
458 end, we collected supernatants from intestinal explants (terminal ileum and distal colon) and
459 analysed the presence of substance P by enzyme immunoassay. The levels of substance P
460 under basal conditions were similar between NMRs and mice (mouse 1.38 ± 2.033 pg
461 substance P · mg $protein^{-1}$ vs. NMR 1.09 ± 1.38 pg substance P · mg $protein^{-1}$, $p > 0.9999$;
462 Figure 7b).

Altogether, these findings indicate that NMRs display a similar hyaluronan localisation along the gut compared to mice, and that basal intestinal levels of substance P are comparable in both species. Further studies will evaluate the distribution of hyaluronan with different molecular weights in the NMR intestine and how this molecule, substance P, and other neuropeptides modulate the gut physiology of these animals.

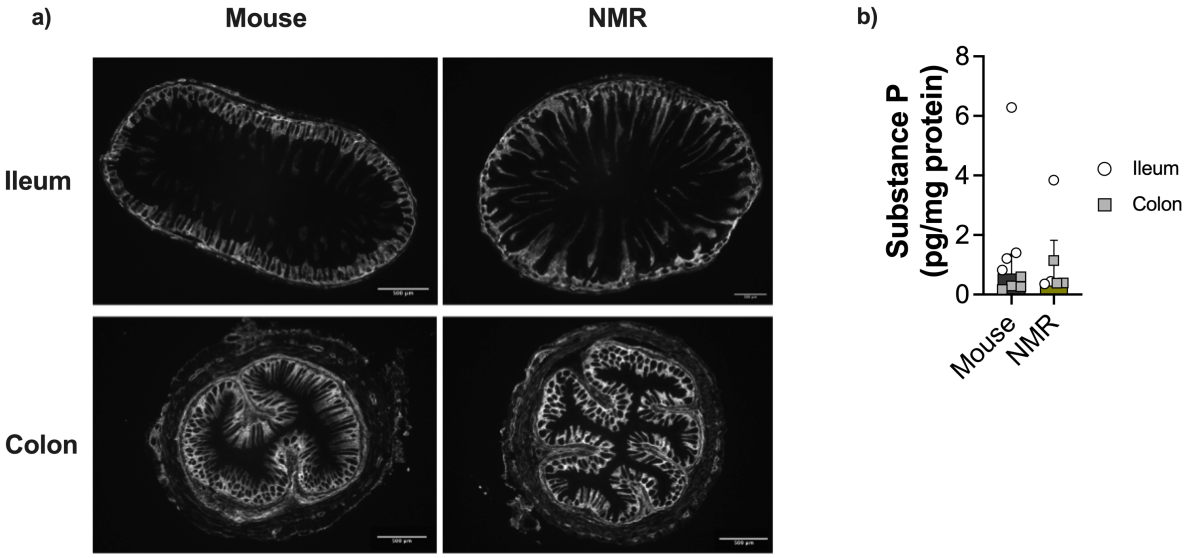

Figure 7. Biomolecules in the gut of NMRs. **a**) Representative images of HABP staining of the terminal ileum of mice (upper left panel) and NMR (upper right panel), and the distal colon of mice (lower left panel) and NMR (lower right panel). Scale bars, 500 µm. **b**) Intestinal levels of substance P (normalised by the content of protein) in mouse (n = 8; 4 ileum samples and 4 colon samples) and NMR (n = 6; 3 ileum samples and 3 colon samples). White circles refer to terminal ileum samples and grey squares to colon samples. **b**, Mann-Whitney test (data shown as median ± IQR).

4. Discussion:

In the present study, we investigated the intestinal barrier function in NMRs as a potential emergent animal model in gastroenterology. Intestinal barrier dysfunction is considered one of the potential underlying pathophysiological mechanisms of many gastrointestinal diseases (*6*), and thus deemed to be of great biological and clinical relevance (*11*). The persisting incidence and prevalence of gastrointestinal conditions in the last decades (*1*) reflects the unmet need for novel strategies in the field. Here, we used NMRs as a non-traditional animal model due to their exceptional biological features (*64*) and studied their intestinal physiology. We found that the NMR small intestine was significantly shorter compared to that of mice, although it displayed a more robust tissue architecture (thicker intestinal layers, longer ileum villi, bigger crypts, and elevated mucus content). In keeping with this, the integrity (measured as TEER by Ussing chambers) of the NMR ileum was remarkably increased compared to the mouse ileum. The colon of NMR, on the other hand, showed more structural similarities to mice, but again displayed enhanced mucus content and superior tissue integrity. Of particular interest, we found that the ileum of NMRs showed reduced anion secretion responses to 5-HT, bradykinin, histamine, and capsaicin, even though receptors for these agonists were expressed in the gastrointestinal tract. Taken together, NMRs represent an animal model of considerable interest for gastroenterology and, particularly, for studying intestinal barrier function.

We first characterised the morphoanatomical features of the intestinal tract in NMRs. The NMR's notably shorter small intestinal length has likely led to the simultaneous development of longer villi compared to those mice, or rats (*65*). NMRs do not drink water and fulfil their hydration requirements entirely through their solid diet. Therefore, we presume that longer villi enable NMRs to increase the surface area to volume ratio for nutrient and water absorption, which has led to water consumption being redundant. In keeping with this, a recent study showed that long villi are found along the entire small bowel of NMR (*23*), as well as enterocytes involved in the digestion and absorption of nutrients and water (*23*, *66*). Furthermore, NMRs exhibited a greater number of goblet cells in the ileum and colon. Additionally, the size of these cells was substantially larger in NMRs and had increased mucus granule content compared to mice. These results strongly suggest that goblet cells in NMRs have an enhanced capacity to produce mucus/mucins. In keeping with this, it was recently reported that NMRs have a thicker mucus layer and elevated expression of *Muc2* (gene encoding for the oligomeric mucus gel-forming protein Mucin 2) compared to mice (*23*), likely conferring an increased protection against environmental chemicals (*23*).

Notably, the histological features of the NMRs small intestine and colon more closely resemble those of bigger rodents, such as rats (*67*) and guinea pigs (*68*, *69*). This is of particular interest because the altered intestinal architecture found in NMRs would not completely explain the increased ileum tissue integrity observed in these animals compared to mice. In fact, previous studies utilising Ussing chambers have reported >2-fold lower TEER values in the ileum of guinea pigs (*70*) and rats (*71*, *72*) compared to our results in NMRs, and similar values in the colon of rats (*71–73*) compared to our findings. This strongly suggests that the small intestine of NMRs possesses strong tight junction structures that increase the integrity of this barrier. In the current study, we measured TEER as a proxy for intestinal integrity, which reflects the net flux of anions and cations across the intestinal barrier, including the contribution of the paracellular resistance (resistance of the tight junctions), the transcellular resistance (resistance to ions of the apical and basolateral membranes), and the subepithelial resistance (*6*). Due to the crucial role of tight junctions (i.e., claudin, occludin, zonula occludens-1, and junctional adhesion molecule-A) to selectively regulate the paracellular flux of ions, the regulation of these barrier components is of great relevance. Future studies will assess the expression, organisation and interprotein interactions of tight junctions in the NMR small intestine and how these control the high-capacity pore pathway (permeable to small ions and small uncharged molecules) and the low-capacity leak pathway (permeable to larger macromolecules) in their intestinal barrier (*74*). Overall, the specific characteristics of the NMR small intestine may represent an interesting model for studying intestinal barrier dysfunction in coeliac disease (*75*) and irritable bowel syndrome (*76*), amongst other conditions. Indeed, we note the interesting results from a recent study showing that NMRs displayed no colonic histological damage, even when exposed to 8.75% DSS, far above the standard 2-3% DSS, albeit for only 3 days (*23*).

Another crucial function of the intestinal barrier is the transport of ions and fluids across the epithelium. Disruption of this well-coordinated process may lead to diarrhoea when the gut's capacity for fluid absorption is exceeded. Of note, we found that the NMR ileum displays reduced anion secretion responses to four different compounds: 5-HT, bradykinin, histamine, and capsaicin. The bradykinin result aligns with our prior observation that this inflammatory mediator fails to activate colonic afferent nerves in NMRs (*41*). However, we did observe that bradykinin led to mechanical sensitisation of these fibres (*41*), suggesting that they express functional bradykinin B_2 receptors. In the present study, we confirmed that NMRs indeed

542 express *Bdkrb2* (gene encoding the bradykinin B_2 receptor) in both the colon and ileum.
543 However, differences in the functionality of these receptors and the downstream effector
544 signalling in NMRs remain to be elucidated. Future studies will also explore the different cells
545 expressing this marker (epithelial cells (*77*) and nerve fibres (*78*)) in NMRs, and how these
546 modulate visceral pain and mucosal ion secretion. The role of 5-HT in the NMR gastrointestinal
547 tract has not been previously characterised. While fibroblasts isolated from the back skin or
548 the lungs of NMRs express high levels of 5-HT (*79*), plasma circulating levels of this
549 neurotransmitter are significantly lower compared to mice (*80*). In the gut, we showed that the
550 anion secretion induced by 5-HT in the ileum was decreased in NMRs compared to mice,
551 although the expression of *Htr4* in this tissue was similar in both species. Further studies are
552 therefore required to determine the functionality of this and other serotonergic receptors, such
553 as 5-HT receptors 1, 2 and 3 (*81*), in different cell types in the NMR intestine. Finally, the lack
554 of cutaneous neuropeptides and unusual connectivity of cutaneous afferent neurons in the
555 spinal cord in NMRs have been proposed to explain the absence capsaicin-induced
556 nocifensive behaviour and associated thermal hypersensitivity (*82*), as well as the lack of
557 histamine-induced scratching behaviour (*83*) in these animals. However, it should be noted
558 that the lack of substance P and CGRP alone cannot completely explain the lack of nocifensive
559 behaviours induced by these compounds, as *Tac1-Calca* double knockout mice (therefore
560 lacking both substance P and CGRPα peptides) display intact responses to mechanical,
561 thermal, chemical, visceral pain, itch, and neurogenic inflammation (*84*). In the present study,
562 we showed that despite the virtually complete absence of anion secretion induced by
563 histamine and capsaicin in NMRs, these animals display intestinal basal levels of substance
564 P comparable to mice. Future studies will investigate the role of substance P and other
565 neurotransmitters/neuropeptides in the gut physiology of NMRs, as well as their cellular
566 sources. Overall, we propose that NMRs may be a promising model for the pathogenesis of
567 inflammation-associated diarrhoea in inflammatory bowel disease (*85*) and serotonin- and
568 histamine-associated diarrhoea in irritable bowel syndrome (*86*, *87*).

569 We recognise that our study has some limitations. Although physiologically age-matched
570 animals for both species were used, intestinal permeability typically changes throughout the
571 lifetime. However, it should be noted that differences in intestinal permeability between mice
572 and NMRs are in the opposite direction of what one would expect, that is, an increased
573 permeability in older animals (*88*). Interestingly, we found that the ileum permeability was
574 similar in young NMRs compared to older animals (young $153.0 \pm 57.09\ \Omega \cdot cm^2$ vs. older
575 $144.2 \pm 42.75\ \Omega \cdot cm^2$, $p = 0.7000$; Supplementary Figure 2c), thus demonstrating that the
576 differences observed between species are not related to age. Furthermore, all NMRs used in
577 the present study were non-breeders and thus we cannot comment on whether or findings
578 would hold true in sexual mature, breeding animals. Sexual maturity is of relevance to our
579 work because it has been shown, for example, that progesterone decreases gut permeability
580 in humans and Caco-2 cells (*89*) and that oestrogen modulates ion secretion in intestinal
581 epithelial cells (*90*). Most of the NMRs used in our study were males (only 1 female was used
582 in TEER experiments and another 1 in short-circuit current experiments), and thus we are
583 unable to draw firm conclusions with regard to any potential sex differences, but being non-
584 breeder animals, all were sexually immature. However, we do not believe that sex and/or state
585 of sexual maturity are likely responsible for the significant differences observed in the NMR
586 ileum, as the relevant hormones would similarly affect the colon, where we found similar TEER
587 values as previously reported in rats (*71–73*). It should be noted as well that the Ussing
588 chambers experiments were performed at 37˚C, that is, 5-7˚C above the NMRs physiological

589 temperature (*91*). However, an increase in the physiological temperature is typically
590 associated with an increase in mucosal permeability (*92*, *93*). It remains to be elucidated
591 whether changes in physiological temperature affect intestinal function in NMRs, although one
592 would normally expect changes in the opposite direction to our findings. Finally, other caveats
593 that must be considered are the differences in diet and microbiota between mice and NMRs,
594 which can affect both the intestinal integrity (*94*) and the anion secretion (*95*). Whether specific
595 gut bacteria found in NMRs (*96*) or compounds of their diet are important to improve intestinal
596 barrier function remain to be elucidated.

597 In conclusion, our work illustrates a remarkably low permeability in the NMR small intestine.
598 Moreover, it reveals that these animals have reduced intestinal anion secretion responses to
599 5-HT, bradykinin, histamine, and capsaicin. Overall, this study adds further evidence to the
600 uncommon biological features exhibited by this species. The NMR gut may therefore offer
601 particular insights into the physiology relevant to gastrointestinal conditions and aid in devising
602 strategies for their treatments. Thus, we strongly support the use of this unconventional animal
603 model in further investigations of intestinal barrier function.

604

605 **5. Acknowledgements:**

606 JA-L and EStJS acknowledge funding from the Medical Research Council (MRC)
607 (MR/W002426/1) and AR was supported by AstraZeneca PhD Studentship (G115018).

608

609 **6. Disclosures:**

610 The authors declare no competing interests.

611

612 **7. Author contribution:**

613 JA-L conceptualised and designed the research study, conducted the experiments (Ussing
614 chamber experiments, gene expression, enzyme immunoassays), acquired and analysed the
615 data and wrote the manuscript. AR conducted the experiments (histology, AB/PAS staining
616 and IHC) and acquired the data. DCB provided experimental support and discussed the data.
617 EStJS provided experimental support, reviewed, and discussed the data and revised the
618 manuscript. All authors corrected and approved the final version of the manuscript.

619

620 **8. Data availability:**

621 Data sets supporting the conclusions of this article are available in University of Cambridge
622 Apollo Repository (http://doi.org/10.17863/CAM.106848).

623

624 **9. ORCID iD:**

625 Javier Aguilera-Lizarraga: https://orcid.org/0000-0002-8135-9933.

626 Anne Ritoux: https://orcid.org/0000-0002-5760-6172

627 David C. Bulmer: https://orcid.org/0000-0002-4703-7877

628 Ewan St. J. Smith: https://orcid.org/0000-0002-2699-1979.

10. References:

1. Y. Wang, Y. Huang, R. C. Chase, T. Li, D. Ramai, S. Li, X. Huang, S. O. Antwi, A. P. Keaveny, M. Pang, Global Burden of Digestive Diseases: A Systematic Analysis of the Global Burden of Diseases Study, 1990 to 2019. *Gastroenterology* **165**, 773-783.e15 (2023).
2. T. C. Rose, A. Pennington, C. Kypridemos, T. Chen, M. Subhani, J. Hanefeld, L. Ricciardiello, B. Barr, Analysis of the burden and economic impact of digestive diseases and investigation of research gaps and priorities in the field of digestive health in the European Region—White Book 2: Executive summary. *United European Gastroenterol J* **10**, 657–662 (2022).
3. V. C. Goodoory, C. E. Ng, C. J. Black, A. C. Ford, Direct healthcare costs of Rome IV or Rome III-defined irritable bowel syndrome in the United Kingdom. *Aliment Pharmacol Ther* **56**, 110–120 (2022).
4. R. S. Sandler, J. E. Everhart, M. Donowitz, E. Adams, K. Cronin, C. Goodman, E. Gemmen, S. Shah, A. Avdic, R. Rubin, The burden of selected digestive diseases in the United States. *Gastroenterology* **122**, 1500–1511 (2002).
5. L. A. Pattison, A. Cloake, S. Chakrabarti, H. Hilton, R. H. Rickman, J. P. Higham, M. Y. Meng, L. W. Paine, L. Qiu, A. Ritoux, D. C. Bulmer, G. Callejo, E. St John Smith, Digging deeper into pain – an ethological behavior assay correlating well-being in mice with human pain experience. *Pain*, doi: 10.1101/2023.08.18.553862 (2024).
6. T. Vanuytsel, J. Tack, R. Farre, The Role of Intestinal Permeability in Gastrointestinal Disorders and Current Methods of Evaluation. *Front Nutr* **8**, 717925 (2021).
7. H. Majamaa, E. Isolauri, Evaluation of the gut mucosal barrier: Evidence for increased antigen transfer in children with atopic eczema. *J Allergy Clin Immunol* **97**, :985-90 (1996).
8. A. Benard, P. Desreumeaux, D. Huglo, A. Hoorelbeke, A.-B. Tonnel, B. Wallaert, iD Lille, Increased intestinal permeability in bronchial asthma. *J Allergy Clin Immunol* **97**, 1173–1181 (1996).
9. A. Fasano, N. P. Visanji, L. W. C. Liu, A. E. Lang, R. F. Pfeiffer, Gastrointestinal dysfunction in Parkinson's disease. Lancet Publishing Group [Preprint] (2015). https://doi.org/10.1016/S1474-4422(15)00007-1.
10. M. P. Fink, Leaky gut hypothesis: a historical perspective. [Preprint] (1990). https://doi.org/10.1097/00003246-199005000-00024.
11. M. Camilleri, Leaky gut: mechanisms, measurement and clinical implications in humans. BMJ Publishing Group [Preprint] (2019). https://doi.org/10.1136/gutjnl-2019-318427.
12. H. Vanheel, M. Vicario, T. Vanuytsel, L. Van Oudenhove, C. Martinez, À. V. Keita, N. Pardon, J. Santos, J. D. Soderholm, J. Tack, R. Farré, Impaired duodenal mucosal integrity and low-grade inflammation in functional dyspepsia. *Gut* **63**, 262–71 (2014).
13. A. Fedi, C. Vitale, G. Ponschin, S. Ayehunie, M. Fato, S. Scaglione, In vitro models replicating the human intestinal epithelium for absorption and metabolism studies: A systematic review. *Journal of Controlled Release* **335**, 247–268 (2021).
14. J. Fogh, T. Orfeo, J. Tiso, F. E. Sharkey, Establishment of human colon carcinoma lines in nude mice. *Exp Cell Biol* **47**, 136–144 (1979).
15. M. González-González, C. Díaz-Zepeda, J. Eyzaguirre-Velásquez, C. González-Arancibia, J. A. Bravo, M. Julio-Pieper, Investigating gut permeability in animal models of disease. Frontiers Media S.A. [Preprint] (2019). https://doi.org/10.3389/fphys.2018.01962.
16. J. Foulke-Abel, J. In, J. Yin, N. C. Zachos, O. Kovbasnjuk, M. K. Estes, H. De Jonge, M. Donowitz, Human Enteroids as a Model of Upper Small Intestinal Ion Transport Physiology and Pathophysiology. *Gastroenterology* **150**, 638-649.e8 (2016).

17. F. Weiß, D. Holthaus, M. Kraft, C. Klotz, M. Schneemann, J. D. Schulzke, S. M. Krug, Human duodenal organoid-derived monolayers serve as a suitable barrier model for duodenal tissue. *Ann N Y Acad Sci* **1515**, 155–167 (2022).
18. A. J. Barker, U. Koch, G. R. Lewin, S. J. Pyott, *The Extraordinary Biology of the Naked Mole-Rat* (2021)vol. 1319.
19. R. Buffenstein, The Naked Mole-Rat: A New Long-Living Model for Human Aging Research. *J Gerontol A Biol Sci Med Sci* **60**, 1369–77 (2005).
20. K. Oka, M. Yamakawa, Y. Kawamura, N. Kutsukake, K. Miura, The Naked Mole-Rat as a Model for Healthy Aging. *Annu Rev Anim Biosci* **11**, 207–226 (2023).
21. G. Maldonado, G. Hernández, Translational control in the naked mole-rat as a model highly resistant to cancer. [Preprint] (2021). https://doi.org/10.1016/j.bbcan.2020.188455.
22. Y. H. Edrey, D. X. Medina, M. Gaczynska, P. A. Osmulski, S. Oddo, A. Caccamo, R. Buffenstein, Amyloid beta and the longest-lived rodent: the naked mole-rat as a model for natural protection from Alzheimer's disease. *Neurobiol Aging* **34**, 2352–60 (2013).
23. S. Montazid, S. Bandyopadhyay, D. W. Hart, N. Gao, B. Johnson, S. G. Thrumurthy, D. J. Penn, B. Wernisch, M. Bansal, P. M. Altrock, F. Rost, P. Gazinska, P. Ziolkowski, B. H. Hayee, Y. Liu, J. Han, A. Tessitore, J. Koth, W. F. Bodmer, J. E. East, N. C. Bennett, I. Tomlinson, S. Irshad, Adult stem cell activity in naked mole rats for long-term tissue maintenance. *Nat Commun* **14**, 8484 (2023).
24. S. Wirtz, V. Popp, M. Kindermann, K. Gerlach, B. Weigmann, S. Fichtner-Feigl, M. F. Neurath, Chemically induced mouse models of acute and chronic intestinal inflammation. *Nat Protoc* **12**, 1295–1309 (2017).
25. T. S. Taylor, P. Konda, S. S. John, D. C. Bulmer, J. R. F. Hockley, E. S. J. Smith, Galanin suppresses visceral afferent responses to noxious mechanical and inflammatory stimuli. *Physiol Rep* **8**, e14326 (2020).
26. S. U. Mondelaers, S. A. Theofanous, M. V. Florens, E. Perna, J. Aguilera-Lizarraga, G. E. Boeckxstaens, M. M. Wouters, W. M. Mondelaers SU, Theofanous SA, Florens MV, Perna E, Aguilera-Lizarraga J, Boeckxstaens GE, S. U. Mondelaers, S. A. Theofanous, M. V. Florens, E. Perna, J. Aguilera-Lizarraga, G. E. Boeckxstaens, M. M. Wouters, Effect of genetic background and postinfectious stress on visceral sensitivity in Citrobacter rodentium-infected mice. *Neurogastroenterology and Motility* **28**, 647–658 (2016).
27. P. Bankhead, M. B. Loughrey, J. A. Fernández, Y. Dombrowski, D. G. McArt, P. D. Dunne, S. McQuaid, R. T. Gray, L. J. Murray, H. G. Coleman, J. A. James, M. Salto-Tellez, P. W. Hamilton, QuPath: Open source software for digital pathology image analysis. *Sci Rep* **7**, 16878 (2017).
28. K. R. Rogers-Broadway, E. Karteris, Amplification efficiency and thermal stability of qPCR instrumentation: Current landscape and future perspectives. *Exp Ther Med* **10**, 1261–1264 (2015).
29. D. Svec, A. Tichopad, V. Novosadova, M. W. Pfaffl, M. Kubista, How good is a PCR efficiency estimate: Recommendations for precise and robust qPCR efficiency assessments. *Biomol Detect Quantif* **3**, 9–16 (2015).
30. N. Eissa, H. Hussein, H. Wang, M. F. Rabbi, C. N. Bernstein, J. E. Ghia, Stability of reference genes for messenger RNA quantification by real-time PCR in mouse dextran sodium sulfate experimental colitis. *PLoS One* **11**, e0156289 (2016).
31. N. Eissa, L. Kermarrec, H. Hussein, C. N. Bernstein, J. E. Ghia, Appropriateness of reference genes for normalizing messenger RNA in mouse 2,4-dinitrobenzene sulfonic acid (DNBS)-induced colitis using quantitative real time PCR. *Sci Rep* **7**, 42427 (2017).
32. F. Wang, J. Wang, D. Liu, Y. Su, Normalizing genes for real-time polymerase chain reaction in epithelial and nonepithelial cells of mouse small intestine. *Anal Biochem* **399**, 211–217 (2010).
33. J. Zhang, Y. Y. Gao, Y. Q. Huang, Q. Fan, X. T. Lu, C. K. Wang, Selection of housekeeping genes for quantitative gene expression analysis in yellow-feathered broilers. *Ital J Anim Sci* **17**, 540–546 (2018).

34. A. B. Nygard, C. B. Jørgensen, S. Cirera, M. Fredholm, Selection of reference genes for gene expression studies in pig tissues using SYBR green qPCR. *BMC Mol Biol* **8** (2007).
35. K. J. Livak, T. D. Schmittgen, Analysis of relative gene expression data using real-time quantitative PCR and the 2(-Delta Delta C(T)) Method. *Methods*, doi: 10.1006/meth.2001.1262 (2001).
36. J. Aguilera-Lizarraga, M. V. Florens, M. F. Viola, P. Jain, L. Decraecker, I. Appeltans, M. Cuende-Estevez, N. Fabre, K. Van Beek, E. Perna, D. Balemans, N. Stakenborg, S. Theofanous, G. Bosmans, S. U. Mondelaers, G. Matteoli, S. Ibiza Martínez, C. Lopez-Lopez, J. Jaramillo-Polanco, K. Talavera, Y. A. Alpizar, T. B. Feyerabend, H. R. Rodewald, R. Farre, F. A. Redegeld, J. Si, J. Raes, C. Breynaert, R. Schrijvers, C. Bosteels, B. N. Lambrecht, S. D. Boyd, R. A. Hoh, D. Cabooter, M. Nelis, P. Augustijns, S. Hendrix, J. Strid, R. Bisschops, D. E. Reed, S. J. Vanner, A. Denadai-Souza, M. M. Wouters, G. E. Boeckxstaens, Local immune response to food antigens drives meal-induced abdominal pain. *Nature* **590**, 151–156 (2021).
37. S. De Schepper, S. Verheijden, J. Aguilera-Lizarraga, M. F. Viola, W. Boesmans, N. Stakenborg, I. Voytyuk, I. Smidt, B. Boeckx, I. Dierckx de Casterlé, V. Baekelandt, E. Dominguez Gonzalez, M. Mack, I. Depoortere, B. De Strooper, B. Sprangers, U. Himmelreich, S. Soenen, M. Guilliams, P. Vanden Berghe, E. Jones, D. Lambrechts, G. Boeckxstaens, Self-Maintaining Gut Macrophages Are Essential for Intestinal Homeostasis. *Cell* **175**, 400-415.e13 (2018).
38. C. Wang, R. Weindruch, J. R. Fernández, C. S. Coffey, P. Patel, D. B. Allison, Caloric restriction and body weight independently affect longevity in Wistar rats. *International journal of obesity and related metabolic disorders: journal of the International Association for the Study of Obesity.* **28**, 357–362 (2004).
39. M. Altun, E. Bergman, E. Edström, H. Johnson, B. Ulfhake, Behavioral impairments of the aging rat. *Physiol Behav* **92**, 911–923 (2007).
40. B. Wiggs, A. Churg, J. L. Wright, Influence of weight on pulmonary function in the adult guinea pig. *Respiration* **58**, 37–41 (1991).
41. J. R. F. Hockley, K. H. Barker, T. S. Taylor, G. Callejo, Z. M. Husson, D. C. Bulmer, E. S. J. Smith, Acid and inflammatory sensitisation of naked mole-rat colonic afferent nerves. *Mol Pain* **16**, 1744806920903150 (2020).
42. F. Treves, Anatomy of the Intestinal Canal and Peritoneum in Man. *British Medical Journal* **1**, 580–583 (1885).
43. B. M. L. Underhill, Intestinal length in man. *British Medical Journal* **2**, 1243–1246 (1955).
44. G. Hounnou, C. Destrieux, J. Desmé, P. Bertrand, S. Velut, Anatomical study of the length of the human intestine. *Surgical and Radiologic Anatomy* **24**, 290–294 (2002).
45. S. Sadahiro, T. Ohmura, Y. Yamada, T. Saito, Y. Taki, Analysis of length and surface area of each segment of the large intestine according to age, sex and physique. *Surg Radiol Anat* **14**, 251–257 (1992).
46. L. T. Weaver, S. Austin, T. J. Cole, M. Dunn, Small intestinal length: a factor essential for gut adaptation. *Gut* **32**, 1321–1323 (1991).
47. N. Hanning, R. Verboven, J. G. De Man, H. Ceuleers, H. U. De Schepper, A. Smet, B. Y. De Winter, Single-day and multi-day exposure to orogastric gavages does not affect intestinal barrier function in mice. *American Journal of Physiology-Gastrointestinal and Liver Physiology* **324**, G281–G294 (2023).
48. L. Feighery, A. Smyth, S. Keely, A. W. Baird, W. T. O'Connor, J. J. Callanan, D. J. Brayden, Increased intestinal permeability in rats subjected to traumatic frontal lobe percussion brain injury. *Journal of Trauma - Injury, Infection and Critical Care* **64**, 131–137 (2008).
49. P. Nejdfors, M. Ekelund, B. Jeppsson, B. R. Weström, Mucosal in vitro permeability in the intestinal tract of the pig, the rat, and man: Species- and region-related differences. *Scand J Gastroenterol* **35**, 501–507 (2000).
50. Å. Sjöberg, M. Lutz, C. Tannergren, C. Wingolf, A. Borde, A. L. Ungell, Comprehensive study on regional human intestinal permeability and prediction of fraction absorbed of

drugs using the Ussing chamber technique. *European Journal of Pharmaceutical Sciences* **48**, 166–180 (2013).

51. M. R. Budhoo, R. P. Harris, J. M. Kellum, 5-Hydroxytryptamine-induced Cl- transport is mediated by 5-HT3 and 5-HT4 receptors in the rat distal colon. *Eur J Pharmacol* **298**, 137–144 (1996).
52. M. R. Budhoo, J. M. Kellum, E. Woltering, S. Ashley, B. Bass, The 5-HT4 receptor mediates 5-hydroxytryptamine-induced rise in short circuit current in the human jejunum in vitro. *Surgery* **116**, 396–400 (1994).
53. A. W. Baird, M. M. Skelly, D. P. O'Donoghue, K. E. Barrett, S. J. Keely, Bradykinin regulates human colonic ion transport in vitro. *Br J Pharmacol* **155**, 558–566 (2008).
54. D. C. Manning, S. H. Snyder, J. F. Kachur, R. J. Miller, M. Field, Bradykinin receptor-mediated chloride secretion in intestinal function. *Nature* **299**, 256–259 (1982).
55. Y. Wang, H. J. Cooke, R. Fertel, H. Su, Histamine augments colonic secretion in guinea pig distal colon. *American journal of physiology* **258**, G432–G439 (1990).
56. G. Schultheiss, B. Hennig, W. Schunack, G. Prinz, M. Diener, Histamine-induced ion secretion across rat distal colon: Involvement of histamine H1 and H2 receptors. *Eur J Pharmacol* **546**, 161–170 (2006).
57. S. Yarrow, J. A. Ferrar, H. M. Cox, The effects of capsaicin upon electrogenic ion transport in rat descending colon. *Naunyn-Schmiedeberg's Arch Pharmacol* **344**, 557–563 (1991).
58. E. Weber, M. Neunlist, M. Schemann, T. Frieling, Neural components of distension-evoked secretory responses in the guinea-pig distal colon. *Journal of Physiology* **536**, 741–751 (2001).
59. S. Garantziotis, R. C. Savani, Hyaluronan biology: A complex balancing act of structure, function, location and context. *Matrix Biology* **78–79**, 1–10 (2019).
60. X. Tian, J. Azpurua, C. Hine, A. Vaidya, M. Myakishev-Rempel, J. Ablaeva, Z. Mao, E. Nevo, V. Gorbunova, A. Seluanov, High-molecular-mass hyaluronan mediates the cancer resistance of the naked mole rat. *Nature* **499**, 346–349 (2013).
61. D. del Marmol, S. Holtze, N. Kichler, A. Sahm, B. Bihin, V. Bourguignon, S. Dogné, K. Szafranski, T. B. Hildebrandt, B. Flamion, Abundance and size of hyaluronan in naked mole-rat tissues and plasma. *Sci Rep* **11**, 7951 (2021).
62. Y. Kulaberoglu, B. Bhushan, F. Hadi, S. Chakrabarti, W. T. Khaled, K. S. Rankin, E. S. J. Smith, D. Frankel, The material properties of naked mole-rat hyaluronan. *Sci Rep* **9**, 6632 (2019).
63. T. J. Park, C. Comer, A. Carol, Y. Lu, H. S. Hong, F. L. Rice, Somatosensory organization and behavior in naked mole-rats: II. Peripheral structures, innervation, and selective lack of neuropeptides associated with thermoregulation and pain. *Journal of Comparative Neurology* **465**, 104–120 (2003).
64. R. Buffenstein, V. Amoroso, B. Andziak, S. Avdieiev, J. Azpurua, A. J. Barker, N. C. Bennett, M. A. Brieño-Enríquez, G. N. Bronner, C. Coen, M. A. Delaney, C. M. Dengler-Crish, Y. H. Edrey, C. G. Faulkes, D. Frankel, G. Friedlander, P. A. Gibney, V. Gorbunova, C. Hine, M. M. Holmes, J. U. M. Jarvis, Y. Kawamura, N. Kutsukake, C. Kenyon, W. T. Khaled, T. Kikusui, J. Kissil, S. Lagestee, J. Larson, A. Lauer, L. A. Lavrenchenko, A. Lee, J. B. Levitt, G. R. Lewin, K. N. Lewis Hardell, T. H. D. Lin, M. J. Mason, D. McCloskey, M. McMahon, K. Miura, K. Mogi, V. Narayan, T. P. O'Connor, K. Okanoya, M. J. O'Riain, T. J. Park, N. J. Place, K. Podshivalova, M. E. Pamenter, S. J. Pyott, J. Reznick, J. G. Ruby, A. B. Salmon, J. Santos-Sacchi, D. K. Sarko, A. Seluanov, A. Shepard, M. Smith, K. B. Storey, X. Tian, E. N. Vice, M. Viltard, A. Watarai, E. Wywial, M. Yamakawa, E. D. Zemlemerova, M. Zions, E. S. J. Smith, The naked truth: a comprehensive clarification and classification of current 'myths' in naked mole-rat biology. *Biological Reviews* **97**, 115–140 (2022).
65. G. E. Holle, Changes in the structure and regeneration mode of the rat small intestinal mucosa following benzalkonium chloride treatment. *Gastroenterology* **101**, 1264–73 (1991).

66. N. Miron, V. Cristea, Enterocytes: Active cells in tolerance to food and microbial antigens in the gut. [Preprint] (2012). https://doi.org/10.1111/j.1365-2249.2011.04523.x.
67. A. Bosi, D. Banfi, M. Bistoletti, L. M. Catizzone, A. M. Chiaravalli, P. Moretto, E. Moro, E. Karousou, M. Viola, M. C. Giron, F. Crema, C. Rossetti, G. Binelli, A. Passi, D. Vigetti, C. Giaroni, A. Baj, Hyaluronan Regulates Neuronal and Immune Function in the Rat Small Intestine and Colonic Microbiota after Ischemic/Reperfusion Injury. *Cells* **11**, 3370 (2022).
68. M. Mitjans, R. Ferrer, Morphometric Study of the Guinea Pig Small Intestine during Development. *Microsc Res Tech* **63**, 206–214 (2004).
69. J. Zhao, D. Liao, J. Yang, H. Gregersen, Biomechanical remodelling of obstructed guinea pig jejunum. *J Biomech* **43**, 1322–1329 (2010).
70. R. Moore, C. Pothoulakis, J. Thomas Lamont, S. Carlson, J. L. Madara, J. L. MADARA C difficile, C. difficile toxin A increases intestinal permeability and induces Cl- secretion. *Am J Physiol* **259**, G165-72 (1990).
71. L. Feighery, A. Smyth, S. Keely, A. W. Baird, W. T. O'Connor, J. J. Callanan, D. J. Brayden, Increased intestinal permeability in rats subjected to traumatic frontal lobe percussion brain injury. *Journal of Trauma - Injury, Infection and Critical Care* **64**, 131–137 (2008).
72. B. I. Polentarutti, A. L. Peterson, À. K. Sjöberg, E. K. I. Anderberg, L. M. Utter, A. L. B. Ungell, Evaluation of viability of excised rat intestinal segments in the Ussing chamber: Investigation of morphology, electrical parameters, and permeability characteristics. *Pharm Res* **16**, 446–54 (1999).
73. A. A. Livanova, A. A. Fedorova, A. V. Zavirsky, I. I. Krivoi, A. G. Markov, Dose- and Segment-Dependent Disturbance of Rat Gut by Ionizing Radiation: Impact of Tight Junction Proteins. *Int J Mol Sci* **24**, 1753 (2023).
74. L. Shen, C. R. Weber, D. R. Raleigh, D. Yu, J. R. Turner, Tight junction pore and leak pathways: A dynamic duo. *Annu Rev Physiol* **73**, 289–309 (2011).
75. R. M. Van Elburg, J. J. Uil, C. J. J. Mulder, H. S. A. Heymans, Intestinal permeability in patients with coeliac disease and relatives of patients with coeliac disease. *Gut* **34**, 354–7 (1993).
76. A. M. González-Castro, C. Martínez, E. Salvo-Romero, M. Fortea, C. Pardo-Camacho, T. Pérez-Berezo, C. Alonso-Cotoner, J. Santos, M. Vicario, Mucosal pathobiology and molecular signature of epithelial barrier dysfunction in the small intestine in irritable bowel syndrome. [Preprint] (2017). https://doi.org/10.1111/jgh.13417.
77. A. W. Baird, M. M. Skelly, D. P. O'Donoghue, K. E. Barrett, S. J. Keely, Bradykinin regulates human colonic ion transport in vitro. *Br J Pharmacol* **155**, 558–66 (2008).
78. J. Yi, Z. Bertels, J. S. Del Rosario, A. J. Widman, R. A. Slivicki, M. Payne, H. M. Susser, B. A. Copits, R. W. Gereau, Bradykinin receptor expression and bradykinin-mediated sensitization of human sensory neurons. *Pain* **165**, 202–215 (2024).
79. Y. Kawamura, K. Oka, T. Semba, M. Takamori, Y. Sugiura, R. Yamasaki, Y. Suzuki, T. Chujo, M. Nagase, Y. Oiwa, S. Fujioka, S. Homma, Y. Yamamura, S. Miyawaki, M. Narita, T. Fukuda, Y. Sakai, T. Ishimoto, K. Tomizawa, M. Suematsu, T. Yamamoto, H. Bono, H. Okano, K. Miura, Cellular senescence induction leads to progressive cell death via the INK4a-RB pathway in naked mole-rats. *EMBO J* **42**, e111133 (2023).
80. K. N. Lewis, N. D. Rubinstein, R. Buffenstein, A window into extreme longevity; the circulating metabolomic signature of the naked mole-rat, a mammal that shows negligible senescence. *Geroscience* **40**, 105–121 (2018).
81. M. B. Hansen, A. B. Witte, The role of serotonin in intestinal luminal sensing and secretion. [Preprint] (2008). https://doi.org/10.1111/j.1748-1716.2008.01870.x.
82. T. J. Park, Y. Lu, R. Jüttner, E. S. J. Smith, J. Hu, A. Brand, C. Wetzel, N. Milenkovic, B. Erdmann, P. A. Heppenstall, C. E. Laurito, S. P. Wilson, G. R. Lewin, Selective inflammatory pain insensitivity in the African naked mole-rat (Heterocephalus glaber). *PLoS Biol* **6**, 0156–0170 (2008).
83. E. S. J. Smith, G. R. C. Blass, G. R. Lewin, T. J. Park, Absence of histamine-induced itch in the African naked mole-rat and "rescue" by Substance P. *Mol Pain* **6**, 29 (2010).

84. D. I. Macdonald, M. Jayabalan, J. Seaman, A. Nickolls, A. Chesler, Pain persists in mice lacking both Substance P and CGRPα signaling. *Elife* **13**, RP93754 (2024).
85. A. N. Anbazhagan, S. Priyamvada, W. A. Alrefai, P. K. Dudeja, Pathophysiology of IBD associated diarrhea. *Tissue Barriers* **6**, e1463897 (2018).
86. W. D. Chey, J. Kurlander, S. Eswaran, Irritable bowel syndrome: A clinical review. American Medical Association [Preprint] (2015). https://doi.org/10.1001/jama.2015.0954.
87. J. D. Wood, Neuropathophysiology of the Irritable Bowel Syndrome. *J Clin Gastroenterol* **35**, S11-22 (2002).
88. N. Thevaranjan, A. Puchta, C. Schulz, A. Naidoo, J. C. Szamosi, C. P. Verschoor, D. Loukov, L. P. Schenck, J. Jury, K. P. Foley, J. D. Schertzer, M. J. Larché, D. J. Davidson, E. F. Verdú, M. G. Surette, D. M. E. Bowdish, Age-Associated Microbial Dysbiosis Promotes Intestinal Permeability, Systemic Inflammation, and Macrophage Dysfunction. *Cell Host Microbe* **21**, 570 (2018).
89. Z. Zhou, C. Bian, Z. Luo, C. Guille, E. Ogunrinde, J. Wu, M. Zhao, S. Fitting, D. L. Kamen, J. C. Oates, G. Gilkeson, W. Jiang, Progesterone decreases gut permeability through upregulating occludin expression in primary human gut tissues and Caco-2 cells. *Sci Rep* **9**, 8367 (2019).
90. X. Yang, Y. Guo, J. He, F. Zhang, X. Sun, S. Yang, H. Dong, Estrogen and estrogen receptors in the modulation of gastrointestinal epithelial secretion. *Oncotarget* **8**, 97683–97692 (2017).
91. V. M. Kovalzon, O. A. Averina, V. A. Minkov, A. A. Petrin, M. Yu. Vysokikh, Unusual Correlation between Rest–Activity and Body Temperature Rhythms in the Naked Mole Rat (Heterocephalus glaber) as Compared to Five Other Mammalian Species. *J Evol Biochem Physiol* **56**, 451–458 (2020).
92. G. P. Lambert, C. V. Gisolfi, D. J. Berg, P. L. Moseley, L. W. Oberley, K. C. Kregel, Selected contribution: Hyperthermia-induced intestinal permeability and the role of oxidative and nitrosative stress. *J Appl Physiol* **92**, 1750–61 (2002).
93. K. Dokladny, P. L. Moseley, T. Y. Ma, Physiologically relevant increase in temperature causes an increase in intestinal epithelial tight junction permeability. *Am J Physiol Gastrointest Liver Physiol* **290**, G204-12 (2006).
94. O. Inczefi, P. Bacsur, T. Resál, C. Keresztes, T. Molnár, The Influence of Nutrition on Intestinal Permeability and the Microbiome in Health and Disease. [Preprint] (2022). https://doi.org/10.3389/fnut.2022.718710.
95. A. C. Engevik, M. A. Engevik, Exploring the impact of intestinal ion transport on the gut microbiota. *Comput Struct Biotechnol J* **19**, 134–144 (2021).
96. T. Debebe, E. Biagi, M. Soverini, S. Holtze, T. B. Hildebrandt, C. Birkemeyer, D. Wyohannis, A. Lemma, P. Brigidi, V. Savkovic, B. König, M. Candela, G. Birkenmeier, Unraveling the gut microbiome of the long-lived naked mole-rat. *Sci Rep* **7**, 9590 (2017).

11. Supplementary information:

Supplementary Table 1. Primer sequences for gene detection by RT-qPCR.

Species	Sequence (5' → 3')	Target marker	NCBI Ref Seq
Mouse	CACCCCCTTGTACCCTTCAC	TATA-box binding protein (*Tbp*)	NM_013684.3
	CAGTTGTCCGTGGCTCTCTT		NM_013684.3
Mouse	CCGGCTCGCTTGAGAAAAGG	Bradykinin receptor β2 (*Bdkrb2*)	NM_009747.2
	CCGACAGAAACCCGAGTAGC		NM_009747.2
Mouse	ACGAGTGAAACCCGATGCTT	Histamine receptor H1 (*Hrh1*)	NM_001252642.3
	CTCTGGCTGTCCTAGGGAGT		NM_001252642.3
Mouse	CCTCACAGCAACTTCTCCTT	5-hydroxytryptamine (serotonin) receptor 4 (*Htr4*)	NM_008313.4
	TCCCCTGACTTCCTCAAATA		NM_008313.4
Mouse	GAGTATGCCCAGAGCCCATC	Transient receptor potential vanilloid 1 (*Trpv1*)	NM_001001445.2
	CAGGCTGCTGTGTGGTAAGA		NM_001001445.2
NMR	TTAATTTCGTTTCCGCGGGC	TATA-box binding protein (*Tbp*)	XM_004868859.3
	GCATAAGGTGGGAGGCTGTT		XM_004868859.3
NMR	CTGGGAGGGAGCTGTAGTCA	Bradykinin receptor β2 (*Bdkrb2*)	XM_021244763.1
	CCTCCTAGGCACTTCCTCCT		XM_021244763.1
NMR	CCCACACGTGGCTTAGAGTT	Histamine receptor H1 (*Hrh1*)	XM_004874845.3
	TTGCTTTGAACATGCAGCCC		XM_004874845.3
NMR	ATGTGGCTCACCACCTTAGC	5-hydroxytryptamine (serotonin) receptor 4 (*Htr4*)	XM_021266180.1
	GTGCCTCATGCCTCACTGAT		XM_021266180.1
NMR	TGTGCAATCGCTGTTCATGC	Transient receptor potential vanilloid 1 (*Trpv1*)	NM_001279859.1
	TGGAAGCCTCGGGTGTAGTA		NM_001279859.1

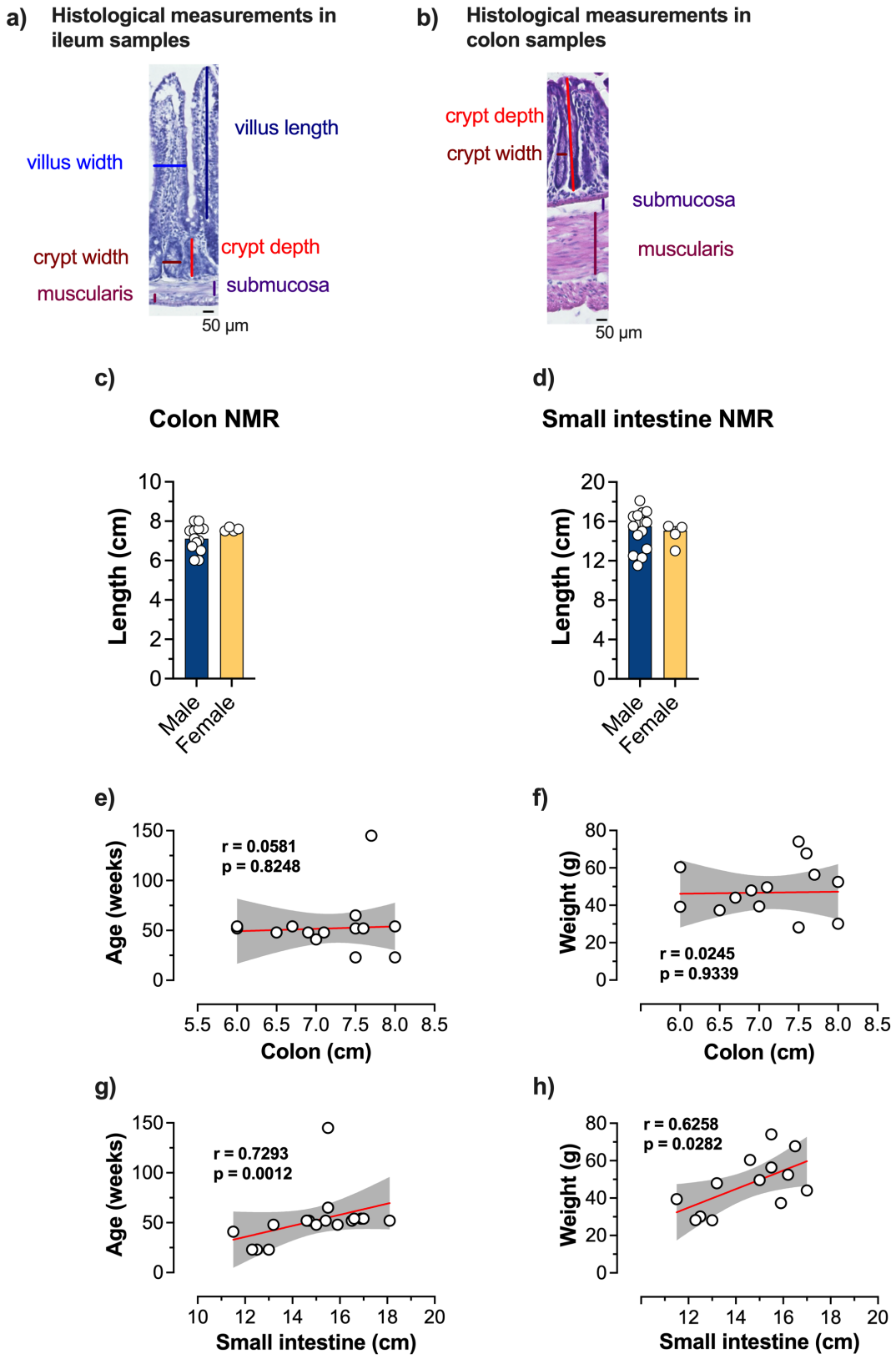

Supplementary Figure 1. Extended anatomical analyses of the NMR gastrointestinal tract. Representative images of the histological measurements performed in ileum (**a**) and colon (**b**) samples. **c)** Colon length in male (n = 13) and female (n = 4) NMRs. **d)** Small intestine length in male (n = 13) and female (n = 4) NMRs. **e)** Correlation between age and colon length in NMRs (n = 17). **f)** Correlation between weight and colon length in NMRs (n = 17). **g)** Correlation between age and small intestine length in NMRs (n = 17). **h)** Correlation between weight and small

intestine length in NMRs (n = 16). *P* values are shown in plots. **c** and **d**, Mann Whitney test (data shown as median ± IQR); **e**, **f**, **g** and **h**, two-tailed Pearson's correlation (data shown as individual data, and 95% CI).

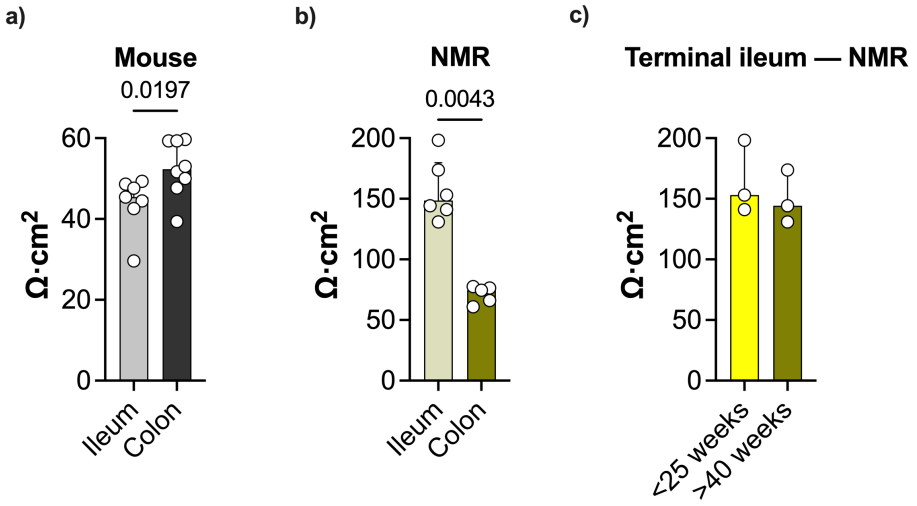

Supplementary Figure 2. Extended analyses of the tissue integrity in NMR and mice. **a)** TEER in the terminal ileum (n = 7) and colon (n = 8) in mice. **b)** TEER in the terminal ileum (n = 6) and colon (n = 5) in NMRs. **c)** TEER in the terminal ileum of young (<25 weeks old; n = 3) and old (>40 weeks old; n = 3) NMRs. Data were calculated as the average TEER values between 60 min and 120 min and plotted as individual values. *P* values are shown in plots. **a**, **b** and **c**, Mann-Whitney test (data shown as median ± IQR).

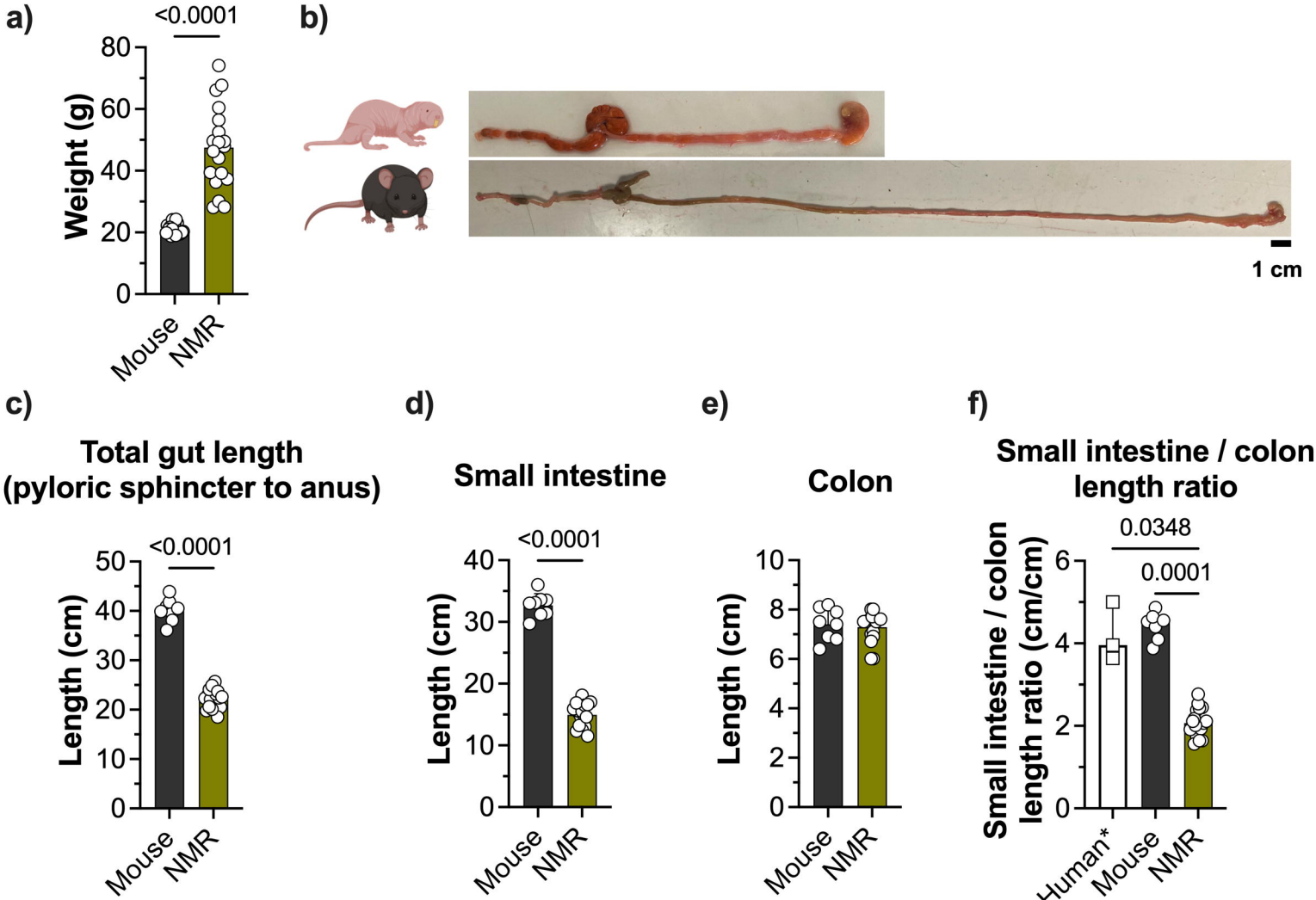
a)
<0.0001
Weight (g)
80
60
40
20
0
Mouse
NMR
b)
1 cm
c)
Total gut length
(pyloric sphincter to anus)
<0.0001
Length (cm)
50
40
30
20
10
0
Mouse
NMR
d)
Small intestine
<0.0001
Length (cm)
40
30
20
10
0
Mouse
NMR
e)
Colon
Length (cm)
10
8
6
4
2
0
Mouse
NMR
f)
Small intestine / colon
length ratio
0.0348
0.0001
Small intestine / colon
length ratio (cm/cm)
6
4
2
0
Human*
Mouse
NMR

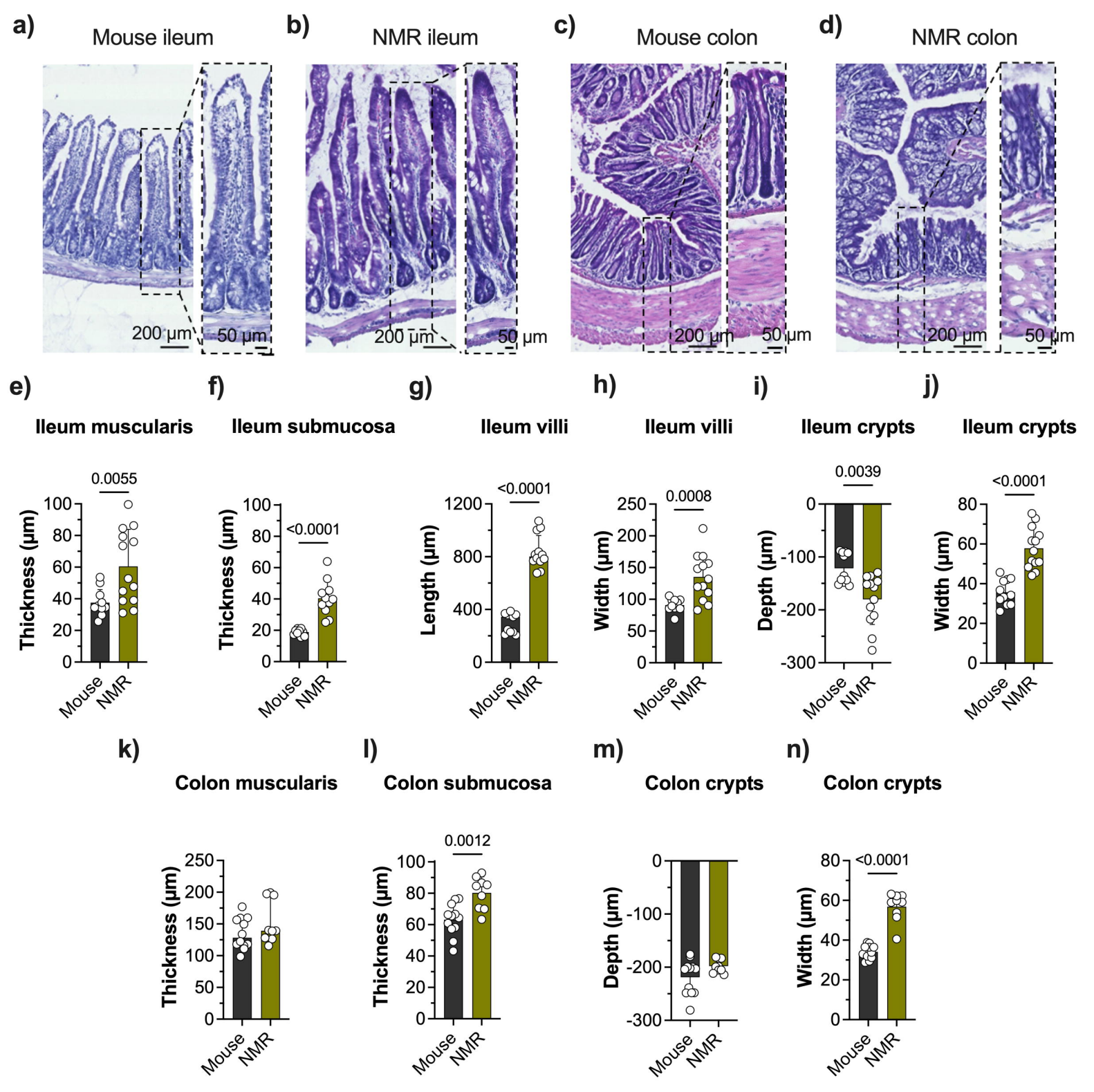
a)
Mouse ileum
200 µm
50 µm
b)
NMR ileum
200 µm
50 µm
c)
Mouse colon
200 µm
50 µm
d)
NMR colon
200 µm
50 µm
e)
Ileum muscularis
Thickness (µm)
0.0055
Mouse
NMR
f)
Ileum submucosa
Thickness (µm)
<0.0001
Mouse
NMR
g)
Ileum villi
Length (µm)
<0.0001
Mouse
NMR
h)
Ileum villi
Width (µm)
0.0008
Mouse
NMR
i)
Ileum crypts
Depth (µm)
0.0039
Mouse
NMR
j)
Ileum crypts
Width (µm)
<0.0001
Mouse
NMR
k)
Colon muscularis
Thickness (µm)
Mouse
NMR
l)
Colon submucosa
Thickness (µm)
0.0012
Mouse
NMR
m)
Colon crypts
Depth (µm)
Mouse
NMR
n)
Colon crypts
Width (µm)
<0.0001
Mouse
NMR

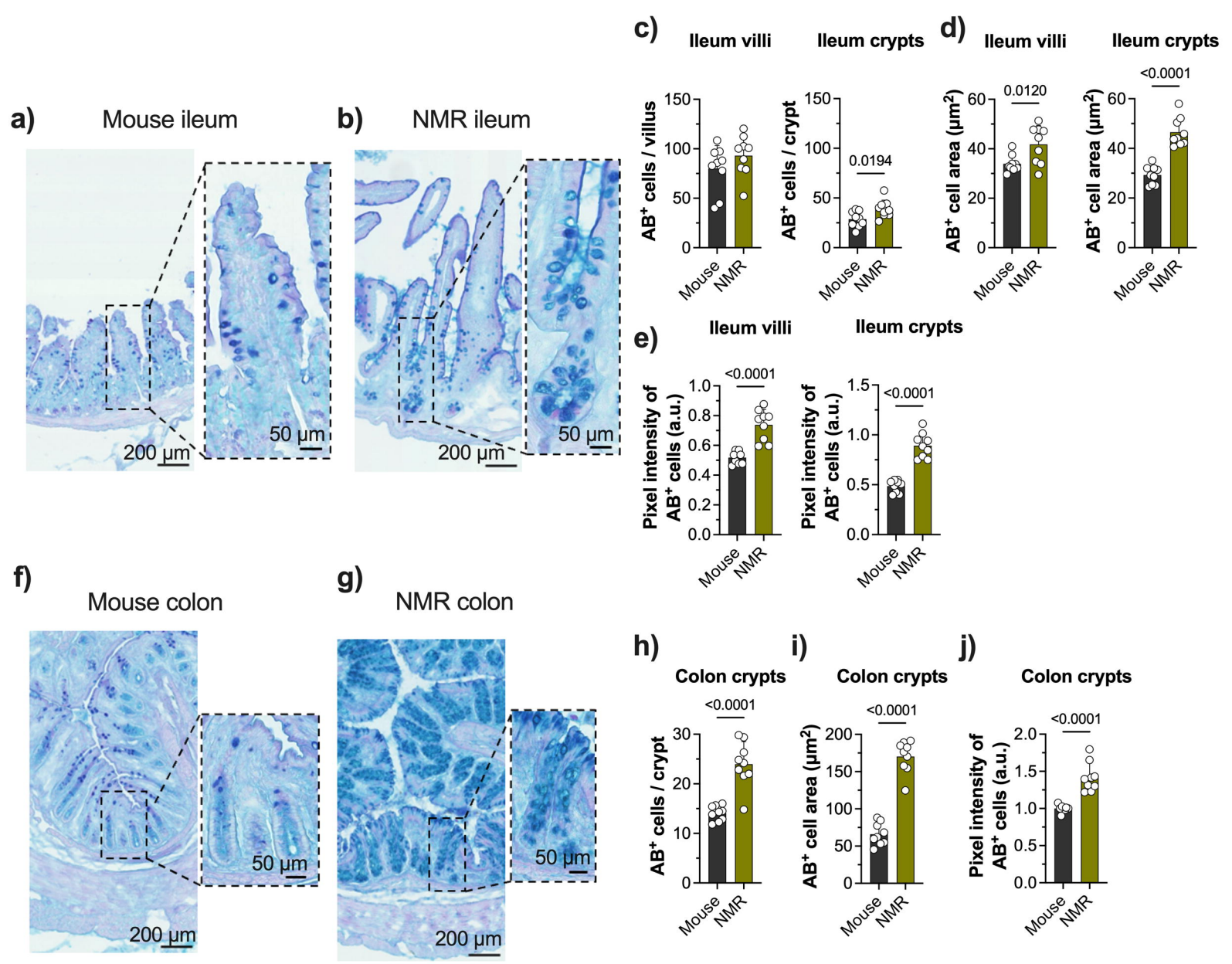
a)
Mouse ileum
200 µm
50 µm
b)
NMR ileum
200 µm
50 µm
c)
Ileum villi
Ileum crypts
AB+ cells / villus
AB+ cells / crypt
0.0194
Mouse
NMR
d)
Ileum villi
Ileum crypts
AB+ cell area (µm2)
0.0120
<0.0001
e)
Ileum villi
Ileum crypts
Pixel intensity of AB+ cells (a.u.)
<0.0001
f)
Mouse colon
200 µm
50 µm
g)
NMR colon
200 µm
50 µm
h)
Colon crypts
AB+ cells / crypt
i)
Colon crypts
AB+ cell area (µm2)
j)
Colon crypts
Pixel intensity of AB+ cells (a.u.)

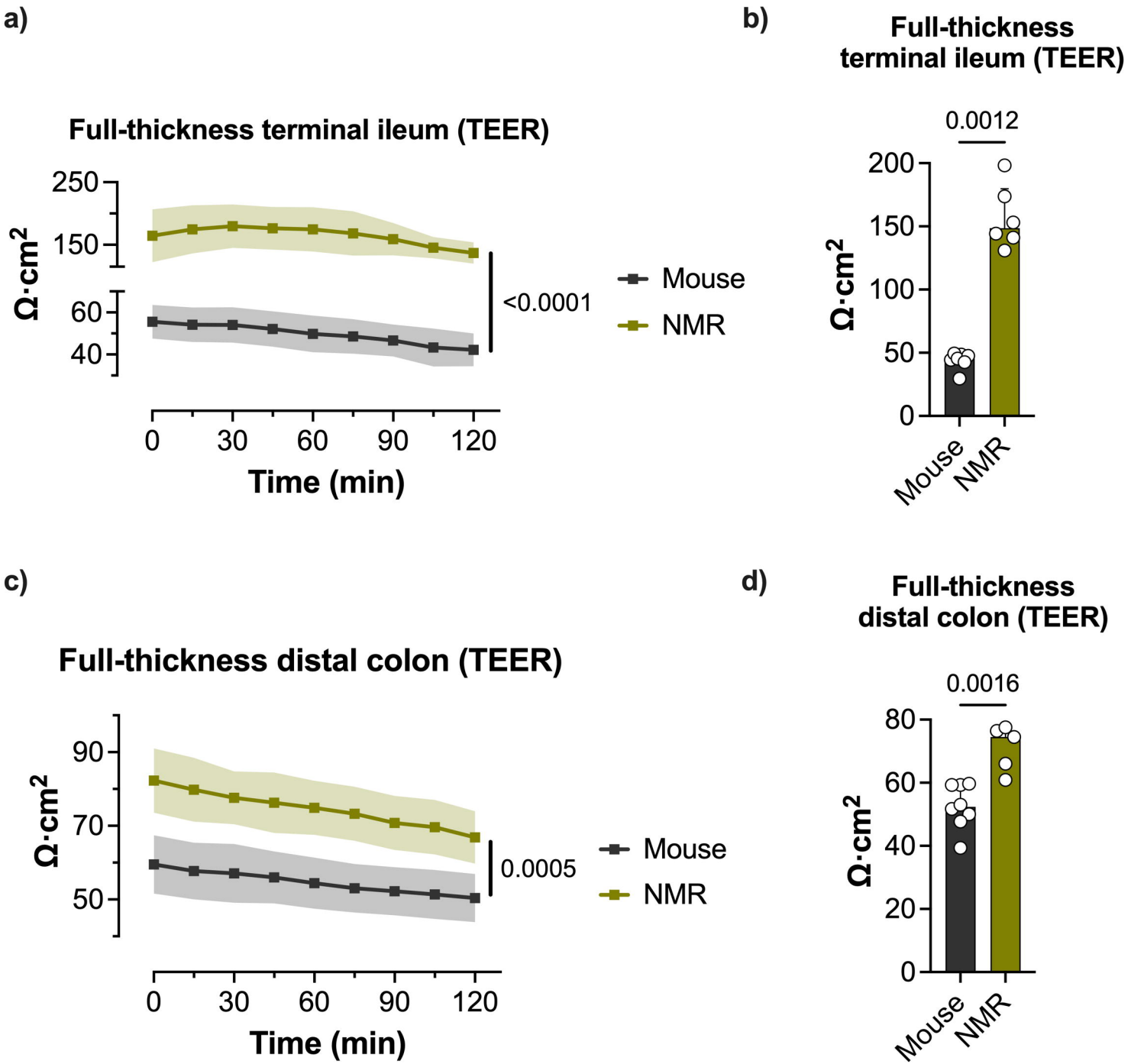
a)
Full-thickness terminal ileum (TEER)
250
150
60
40
Ω·cm2
<0.0001
Mouse
NMR
0
30
60
90
120
Time (min)
b)
Full-thickness terminal ileum (TEER)
0.0012
200
150
100
50
0
Ω·cm2
Mouse
NMR
c)
Full-thickness distal colon (TEER)
90
70
50
Ω·cm2
0.0005
Mouse
NMR
0
30
60
90
120
Time (min)
d)
Full-thickness distal colon (TEER)
0.0016
80
60
40
20
0
Ω·cm2
Mouse
NMR

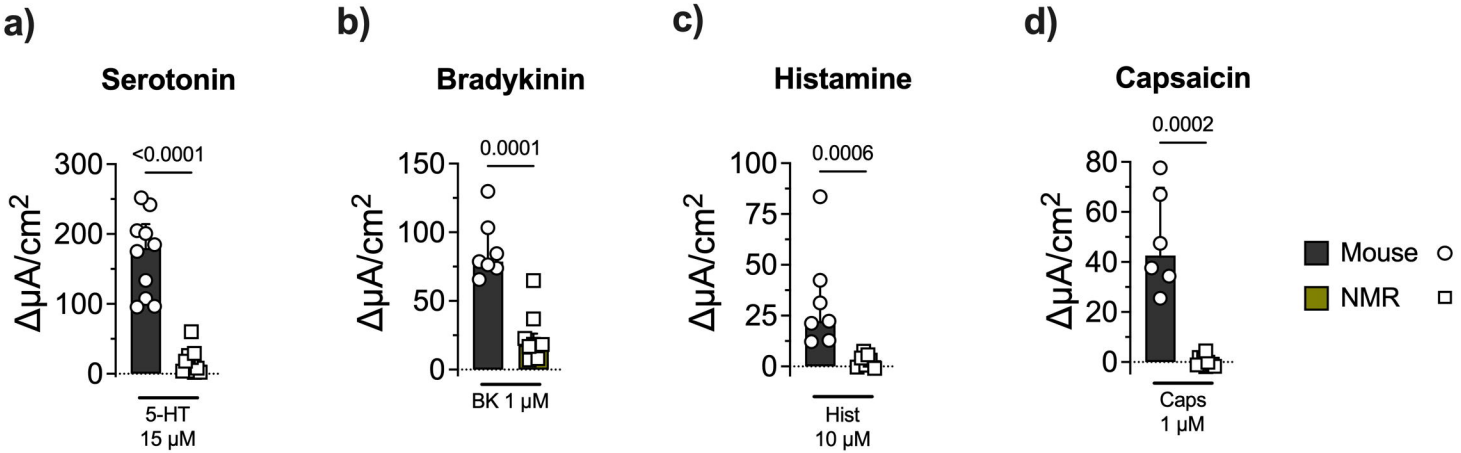
a)
Serotonin
<0.0001
300
200
100
0
ΔμA/cm2
5-HT
15 μM
b)
Bradykinin
0.0001
150
100
50
0
ΔμA/cm2
BK 1 μM
c)
Histamine
0.0006
100
75
50
25
0
ΔμA/cm2
Hist
10 μM
d)
Capsaicin
0.0002
80
60
40
20
0
ΔμA/cm2
Caps
1 μM
Mouse
NMR

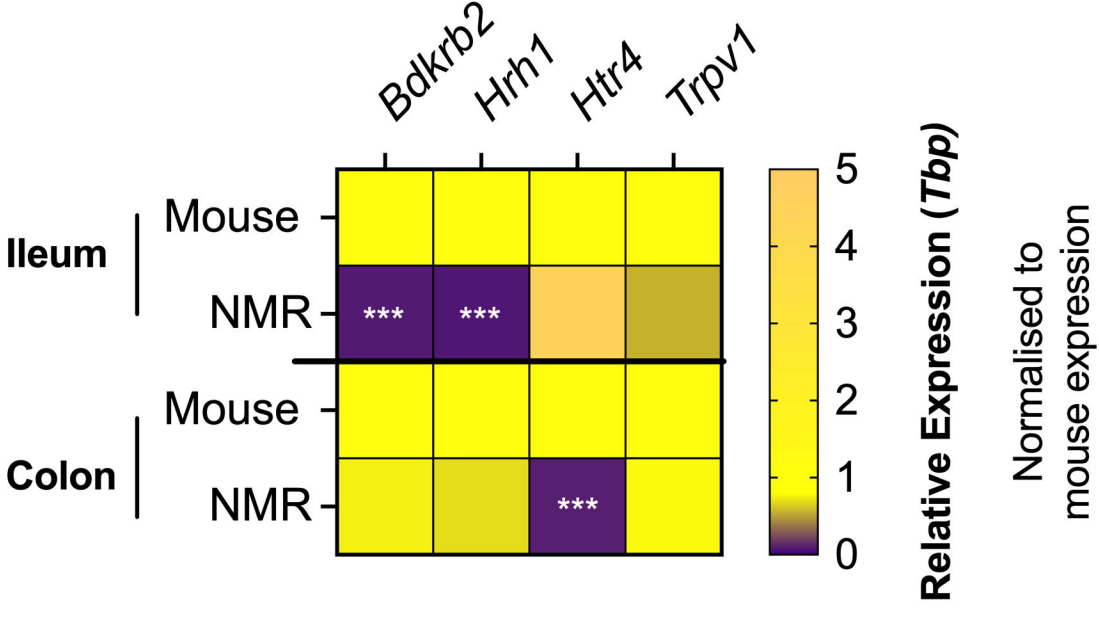
Bdkrb2
Hrh1
Htr4
Trpv1
Ileum
Mouse
NMR
Colon
Mouse
NMR
***
***
***
5
4
3
2
1
0
Relative Expression (Tbp)
Normalised to mouse expression

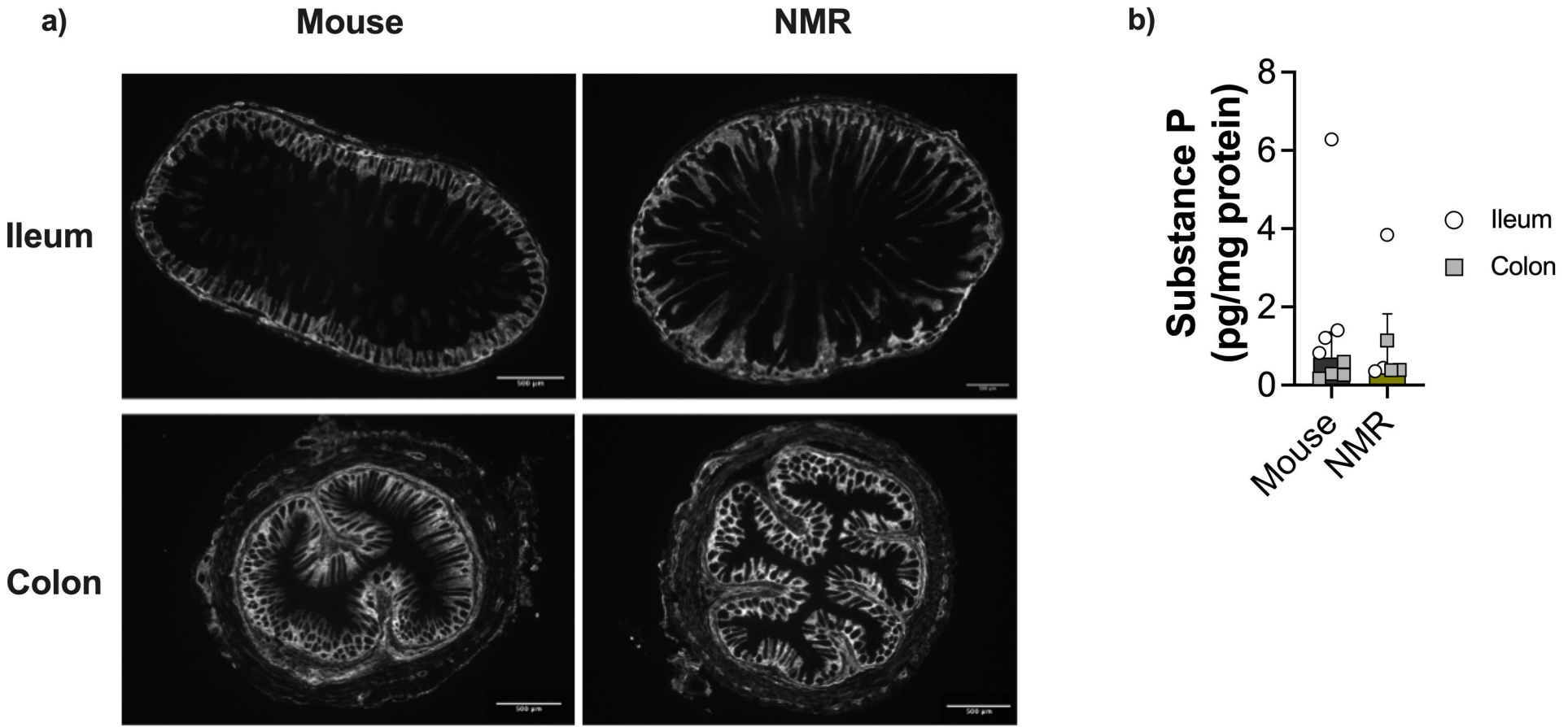
a)
Mouse
NMR
Ileum
Colon
b)
Substance P
(pg/mg protein)
8
6
4
2
0
Mouse
NMR
Ileum
Colon

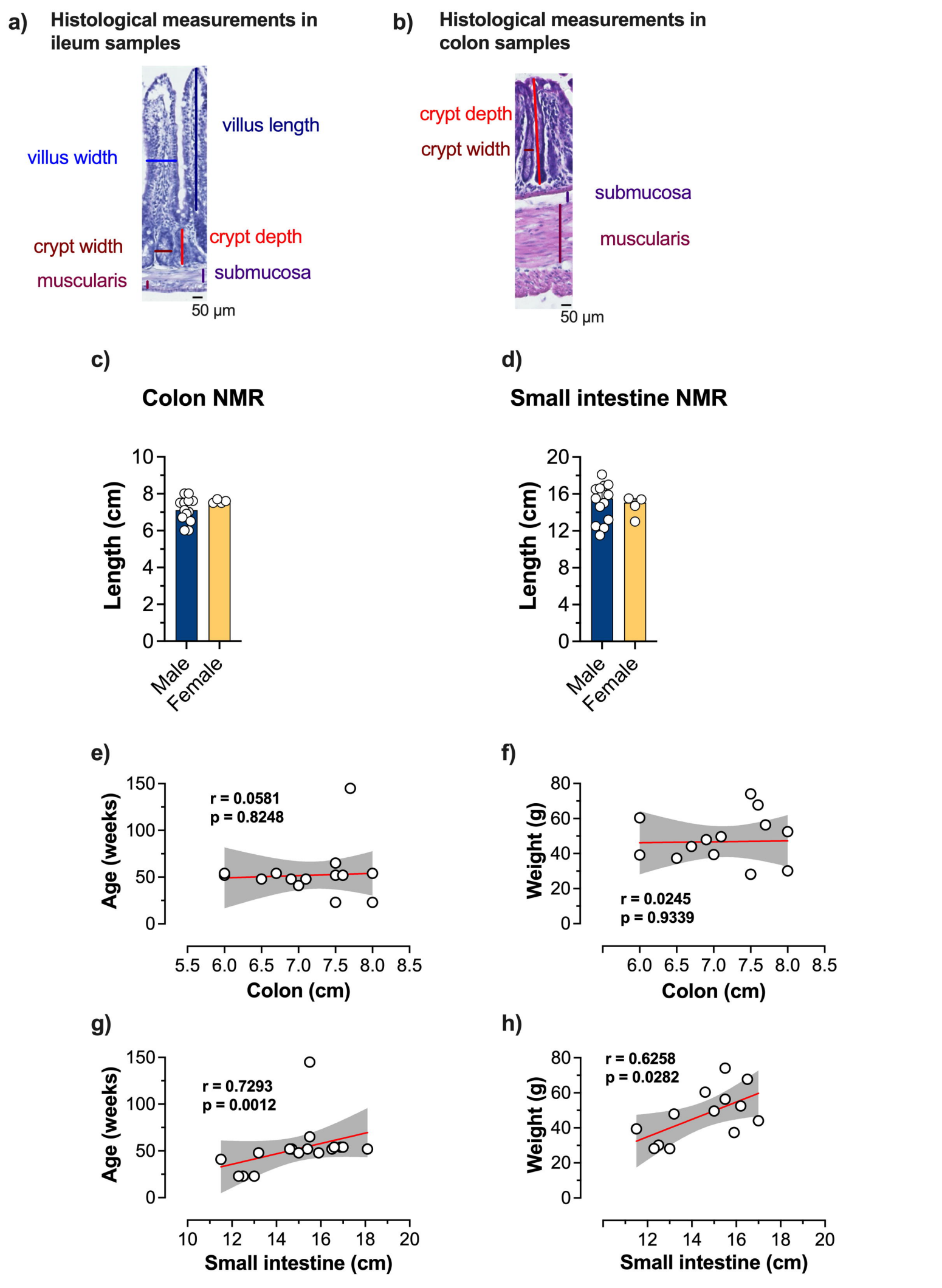
a)
Histological measurements in ileum samples
villus length
villus width
crypt depth
crypt width
submucosa
muscularis
50 µm
b)
Histological measurements in colon samples
crypt depth
crypt width
submucosa
muscularis
50 µm
c)
Colon NMR
Length (cm)
Male
Female
d)
Small intestine NMR
Length (cm)
Male
Female
e)
r = 0.0581
p = 0.8248
Age (weeks)
Colon (cm)
f)
r = 0.0245
p = 0.9339
Weight (g)
Colon (cm)
g)
r = 0.7293
p = 0.0012
Age (weeks)
Small intestine (cm)
h)
r = 0.6258
p = 0.0282
Weight (g)
Small intestine (cm)

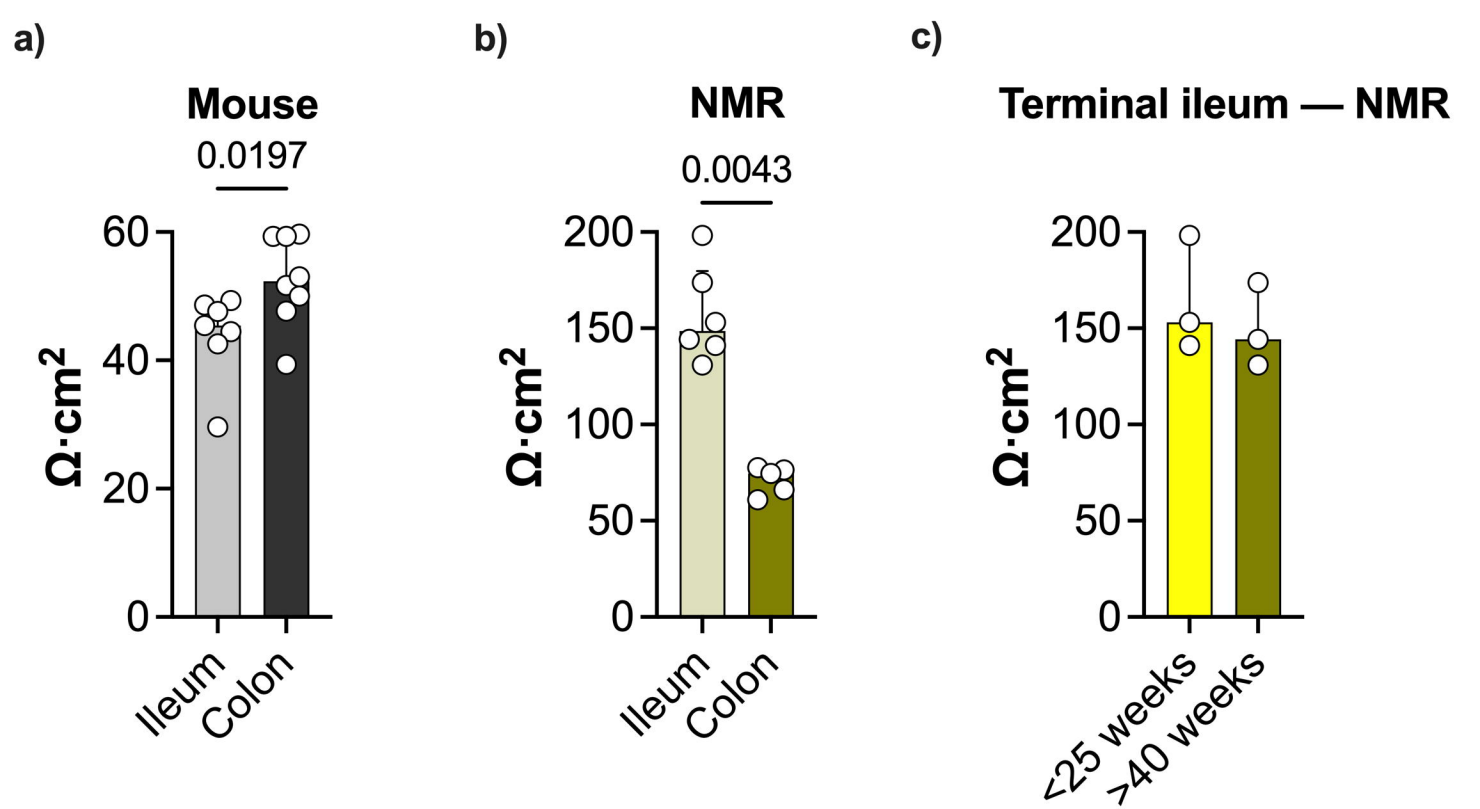
a)
Mouse
0.0197
60
40
20
0
Ω·cm2
Ileum
Colon
b)
NMR
0.0043
200
150
100
50
0
Ω·cm2
Ileum
Colon
c)
Terminal ileum — NMR
200
150
100
50
0
Ω·cm2
<25 weeks
>40 weeks